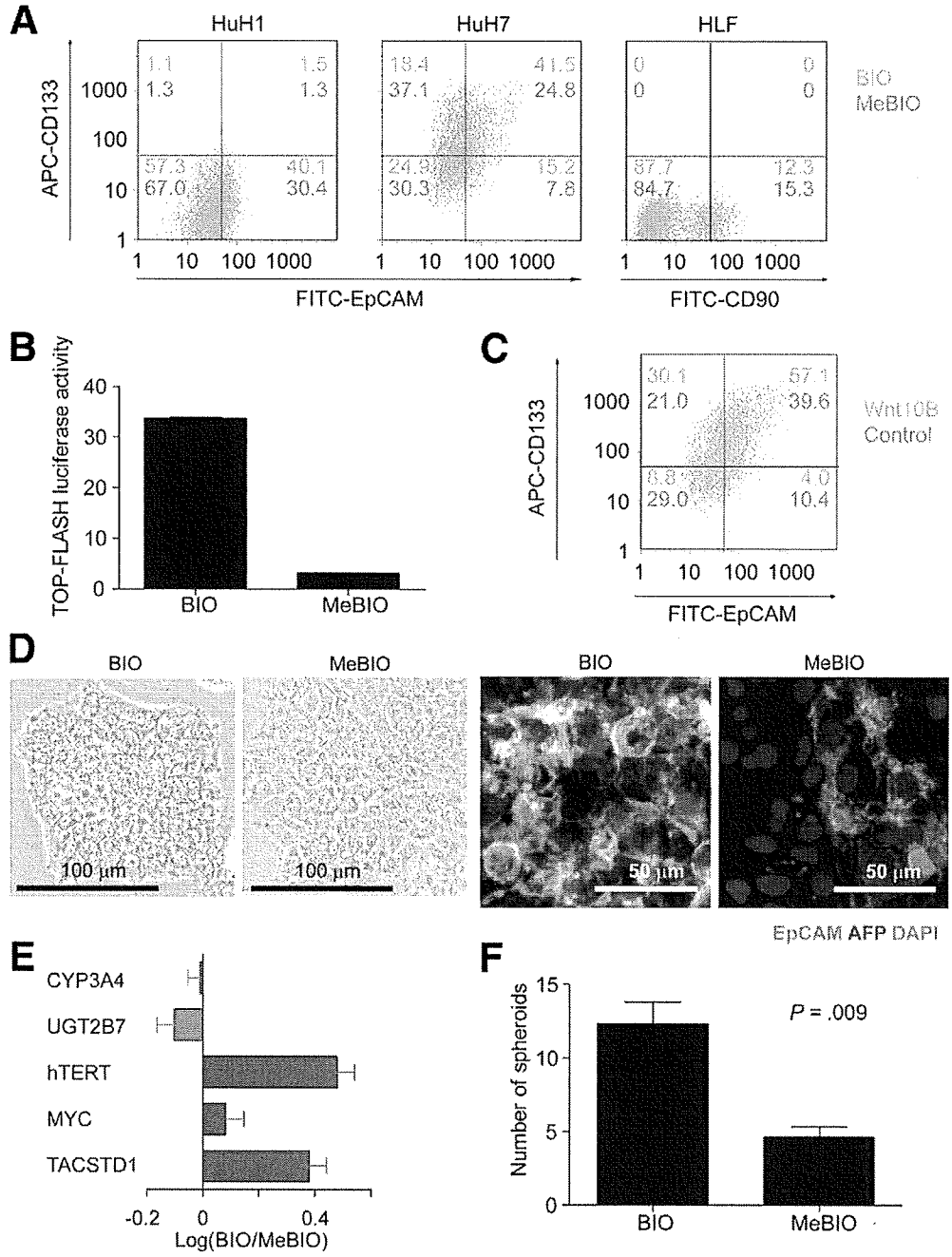

Figure 6. Wnt/β-catenin signaling augments EpCAM+ HCC cells. (*A*) Flow cytometer analysis of HuH1, HuH7, and HLF cells treated with 2 μmol/L of BIO (*orange*) or MeBIO (*green*) for 10 days and stained with anti-EpCAM, anti-CD133 and anti-CD90 antibodies. (*B*) TOP-FLASH luciferase assays of HuH7 cells treated with 2 μmol/L of BIO or MeBIO. (*C*) Flow cytometer analysis of HuH7 cells cultured in normal media (Dulbecco's modified Eagle medium supplemented with 10% FBS) or Wnt10B conditioned media (details are described in the Materials and Methods section). Cells were cultured in each medium for 2 weeks. (*D*) Representative phase-contrast images (*left panel*: *scale bar*, 100 μm) or IF images (*right panel*: *scale bar*, 50 μm) of HuH7 cells treated with 2 μmol/L of BIO or MeBIO for 14 days. (*E*) Quantitative reverse transcription-polymerase chain reaction analysis of representative HpSC-HCC–related genes in HuH7 cells treated with 2 μmol/L of BIO or MeBIO for 14 days. (*F*) Spheroid formation assay of HuH7 cells treated with 2 μmol/L of BIO or MeBIO for 14 days (mean ± SD). FITC, fluorescein isothiocyanate.

to maintain HCC stemness and serve as a good marker for HCC initiating cells.

CD133 or CD90 have been used to identify potential hepatic CSCs.[35,42] CD133 is expressed in normal and malignant stem cells of the neural, hematopoietic, epithelial, hepatic, and endothelial lineages,[23,43,44] suggesting that CD133 is also a common marker to detect normal cells and CSCs. Captivatingly, EpCAM expression overlaps with CD133 expression in normal human colon tissues and colorectal cancer tissues, yet CD133+ and CD133− cells are equally tumorigenic.[45] Similarly, we found that EpCAM+ and EpCAM− HuH1 cells equally expressed CD133, but only EpCAM+ cells developed large hypervascular tumors. Our data suggest that EpCAM may be a better marker than CD133 to enrich HCC tumor-initiating cells from AFP+ tumors. We also found that CD90 expression was limited to HCC cell lines that are EpCAM− AFP−, and Wnt/β-catenin signaling had little effect on CD90+ cell enrichment. These results suggest that the expression patterns of various stem cell markers in tumor-initiating cells with stem/progenitor cell features may be different in each HCC subtype, possibly owing to the heterogeneity of activated signaling pathways in normal stem/progenitor cells where these tumor-initiating cells may originate. Therefore, it would be useful to

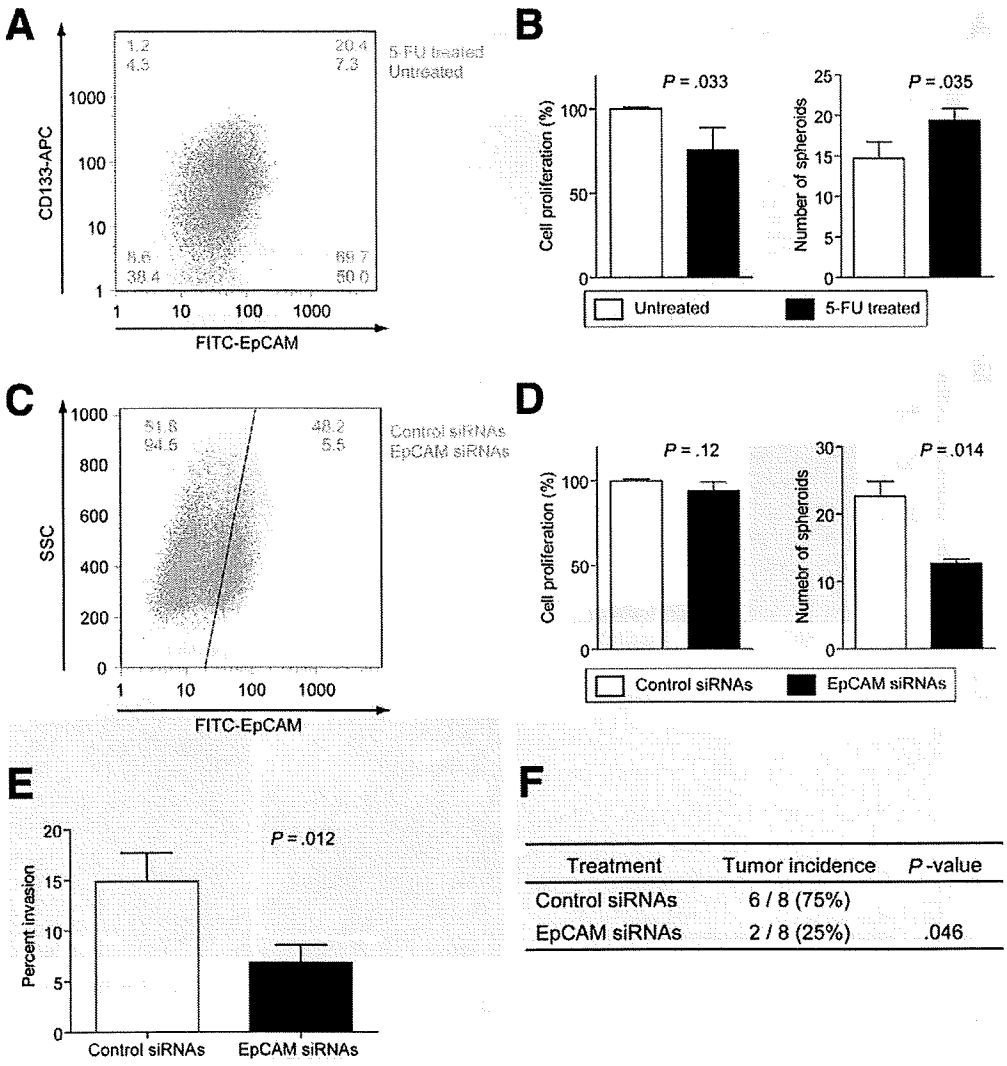

F

Treatment	Tumor incidence	P-value
Control siRNAs	6 / 8 (75%)	
EpCAM siRNAs	2 / 8 (25%)	.046

Figure 7. EpCAM blockage inhibits the tumorigenic and invasive capacity of EpCAM$^+$ HCC cells. (*A*) Enrichment of EpCAM$^+$ cells after 5-FU treatment. HuH1 cells refer as control or without treatment (*green*) or treated with 2 μg/mL of 5-FU (*orange*) for 3 days and analyzed by FACS using anti-EpCAM and anti-CD133 antibodies. (*B*) Spheroid formation of HuH1 cells treated with 2 μg/mL of 5-FU for 3 days. (*C*) FACS analysis of HuH1 cells treated with a control siRNA (orange) or EpCAM-specific siRNA (*green*) at day 3 after transfection. (*D*) Spheroid formation or (*E*) invasive capacity ofEpCAM$^+$ HuH1 cells transfected with a control siRNA or EpCAM-specific siRNA. Experiments were performed in triplicate and the data are shown as mean ± SD. (*D*) siRNAs. (*F*) Inhibition of tumor formation in vivo by EpCAM gene silencing. EpCAM$^+$ HuH1 cells were transfected with siRNA oligos and 1000 cells were injected 24 hours after transfection.

comprehensively investigate the expression patterns of stem cell markers to characterize the population of CSCs that may correlate with the activation of their distinct molecular pathways.

CSCs may be more resistant to chemotherapeutic agents than differentiated tumor cells possibly owing to an increased expression of adenosine triphosphate–binding cassette transporters and anti-apoptotic proteins.[4] Thus, the development of an effective strategy to target CSC pools together with conventional chemotherapies is essential to eradicate a tumor mass.[14] By blocking the programs that activate self-renewal and/or inhibit asymmetric division, CSC features could be destemmed.[46,47] Consistently, EpCAM blockage could inhibit cellular invasion and tumorigenicity of EpCAM$^+$ HCC cells, revealing the feasibility of targeting a CSC marker to destem CSC features. EpCAM may induce c-Myc,[48] a common molecular node activated in HpSC-HCC.[27] c-Myc, together with Oct3/4, Sox2, and Klf4, can induce pluripotent stem cells from adult fibroblasts.[49] It is possible that EpCAM blockage to inhibit hepatic CSCs may result in a suppression of c-Myc signaling. Encouragingly, EpCAM-specific antibodies are currently in phase II clinical trials.[50] Furthermore, a recent study indicated that EpCAM$^+$ circulating tumor cells identified by a unique microfluidic platform can be used to monitor outcomes of patients undergoing systemic treatment.[51] Therefore, it may be useful to combine EpCAM antibodies with conventional chemotherapy to target both CSCs and non-CSCs for the treatment of HCC.

Supplementary Data

Note: To access the supplementary material accompanying this article, visit the online version of *Gastroenterology* at www.gastrojournal.org, and at doi: 10.1053/j.gastro.2008.12.004.

References

1. Fialkow PJ. Clonal origin of human tumors. Biochim Biophys Acta 1976;458:283–321.

2. Heppner GH. Tumor heterogeneity. Cancer Res 1984;44:2259–2265.
3. Hanahan D, Weinberg RA. The hallmarks of cancer. Cell 2000; 100:57–70.
4. Jordan CT, Guzman ML, Noble M. Cancer stem cells. N Engl J Med 2006;355:1253–1261.
5. Clarke MF, Dick JE, Dirks PB, et al. Cancer stem cells—perspectives on current status and future directions: AACR Workshop on cancer stem cells. Cancer Res 2006;66:9339–9344.
6. Potter VR. Phenotypic diversity in experimental hepatomas: the concept of partially blocked ontogeny. The 10th Walter Hubert Lecture. Br J Cancer 1978;38:1–23.
7. Sell S. Cellular origin of cancer: dedifferentiation or stem cell maturation arrest? Environ Health Perspect 1993;101(Suppl 5): 15–26.
8. Wicha MS, Liu S, Dontu G. Cancer stem cells: an old idea—a paradigm shift. Cancer Res 2006;66:1883–1890.
9. Al Hajj M, Wicha MS, Benito-Hernandez A, et al. Prospective identification of tumorigenic breast cancer cells. Proc Natl Acad Sci U S A 2003;100:3983–3988.
10. Singh SK, Hawkins C, Clarke ID, et al. Identification of human brain tumour initiating cells. Nature 2004;432:396–401.
11. Bonnet D, Dick JE. Human acute myeloid leukemia is organized as a hierarchy that originates from a primitive hematopoietic cell. Nat Med 1997;3:730–737.
12. Ricci-Vitiani L, Lombardi DG, Pilozzi E, et al. Identification and expansion of human colon-cancer-initiating cells. Nature 2007; 445:111–115.
13. O'Brien CA, Pollett A, Gallinger S, et al. A human colon cancer cell capable of initiating tumour growth in immunodeficient mice. Nature 2007;445:106–110.
14. Dean M, Fojo T, Bates S. Tumour stem cells and drug resistance. Nat Rev Cancer 2005;5:275–284.
15. Rich JN. Cancer stem cells in radiation resistance. Cancer Res 2007;67:8980–8984.
16. Parkin DM, Bray F, Ferlay J, et al. Global cancer statistics, 2002. CA Cancer J Clin 2005;55:74–108.
17. Sell S, Pierce GB. Maturation arrest of stem cell differentiation is a common pathway for the cellular origin of teratocarcinomas and epithelial cancers. Lab Invest 1994;70:6–22.
18. Thorgeirsson SS, Grisham JW. Hepatic stem cells. Semin Liver Dis 2003;23:301.
19. Thorgeirsson SS, Grisham JW. Molecular pathogenesis of human hepatocellular carcinoma. Nat Genet 2002;31:339–346.
20. Lee JS, Heo J, Libbrecht L, et al. A novel prognostic subtype of human hepatocellular carcinoma derived from hepatic progenitor cells. Nat Med 2006;12:410–416.
21. Sigal SH, Brill S, Fiorino AS, et al. The liver as a stem cell and lineage system. Am J Physiol 1992;263:G139–G148.
22. Schmelzer E, Wauthier E, Reid LM. The phenotypes of pluripotent human hepatic progenitors. Stem Cells 2006;24:1852–1858.
23. Schmelzer E, Zhang L, Bruce A, et al. Human hepatic stem cells from fetal and postnatal donors. J Exp Med 2007;204:1973–1987.
24. Dan YY, Riehle KJ, Lazaro C, et al. Isolation of multipotent progenitor cells from human fetal liver capable of differentiating into liver and mesenchymal lineages. Proc Natl Acad Sci U S A 2006;103:9912–9917.
25. Zaret KS. Regulatory phases of early liver development: paradigms of organogenesis. Nat Rev Genet 2002;3:499–512.
26. Shafritz DA, Oertel M, Menthena A, et al. Liver stem cells and prospects for liver reconstitution by transplanted cells. Hepatology 2006;43:S89–S98.
27. Yamashita T, Forgues M, Wang W, et al. EpCAM and alpha-fetoprotein expression defines novel prognostic subtypes of hepatocellular carcinoma. Cancer Res 2008;68:1451–1461.
28. Reya T, Clevers H. Wnt signalling in stem cells and cancer. Nature 2005;434:843–850.
29. Yamashita T, Budhu A, Forgues M, et al. Activation of hepatic stem cell marker EpCAM by Wnt-β-catenin signaling in hepatocellular carcinoma. Cancer Res 2007;67:10831–10839.
30. Budhu A, Forgues M, Ye QH, et al. Prediction of venous metastases, recurrence and prognosis in hepatocellular carcinoma based on a unique immune response signature of the liver microenvironment. Cancer Cell 2006;10:99–111.
31. Ye QH, Qin LX, Forgues M, et al. Predicting hepatitis B virus-positive metastatic hepatocellular carcinomas using gene expression profiling and supervised machine learning. Nat Med 2003;9:416–423.
32. Wu CG, Forgues M, Siddique S, et al. SAGE transcript profiles of normal primary human hepatocytes expressing oncogenic hepatitis B virus X protein. FASEB J 2002;16:1665–1667.
33. Kubota H, Reid LM. Clonogenic hepatoblasts, common precursors for hepatocytic and biliary lineages, are lacking classical major histocompatibility complex class I antigen. Proc Natl Acad Sci U S A 2000;97:12132–12137.
34. Yoshikawa H, Matsubara K, Zhou X, et al. WNT10B functional dualism: beta-catenin/Tcf-dependent growth promotion or independent suppression with deregulated expression in cancer. Mol Biol Cell 2007;18:4292–4303.
35. Yang ZF, Ho DW, Ng MN, et al. Significance of CD90(+) cancer stem cells in human liver cancer. Cancer Cell 2008;13:153–166.
36. Dontu G, Abdallah WM, Foley JM, et al. In vitro propagation and transcriptional profiling of human mammary stem/progenitor cells. Genes Dev 2003;17:1253–1270.
37. Fang D, Nguyen TK, Leishear K, et al. A tumorigenic subpopulation with stem cell properties in melanomas. Cancer Res 2005; 65:9328–9337.
38. Sato N, Meijer L, Skaltsounis L, et al. Maintenance of pluripotency in human and mouse embryonic stem cells through activation of Wnt signaling by a pharmacological GSK-3-specific inhibitor. Nat Med 2004;10:55–63.
39. Balzar M, Winter MJ, de Boer CJ, et al. The biology of the 17-1A antigen (Ep-CAM). J Mol Med 1999;77:699–712.
40. Trzpis M, McLaughlin PM, de Leij LM, et al. Epithelial cell adhesion molecule: more than a carcinoma marker and adhesion molecule. Am J Pathol 2007;171:386–395.
41. Dalerba P, Dylla SJ, Park IK, et al. Phenotypic characterization of human colorectal cancer stem cells. Proc Natl Acad Sci U S A 2007;104:10158–10163.
42. Ma S, Chan KW, Hu L, et al. Identification and characterization of tumorigenic liver cancer stem/progenitor cells. Gastroenterology 2007;132:2542–2556.
43. Yin AH, Miraglia S, Zanjani ED, et al. AC133, a novel marker for human hematopoietic stem and progenitor cells. Blood 1997;90: 5002–5012.
44. Fargeas CA, Corbeil D, Huttner WB. AC133 antigen, CD133, prominin-1, prominin-2, etc.: prominin family gene products in need of a rational nomenclature. Stem Cells 2003;21:506–508.
45. Shmelkov SV, Butler JM, Hooper AT, et al. CD133 expression is not restricted to stem cells, and both CD133+ and CD133- metastatic colon cancer cells initiate tumors. J Clin Invest 2008; 118:2111–2120.
46. Hill RP, Perris R. "Destemming" cancer stem cells. J Natl Cancer Inst 2007;99:1435–1440.
47. Piccirillo SG, Reynolds BA, Zanetti N, et al. Bone morphogenetic proteins inhibit the tumorigenic potential of human brain tumour-initiating cells. Nature 2006;444:761–765.
48. Munz M, Kieu C, Mack B, et al. The carcinoma-associated antigen EpCAM upregulates c-myc and induces cell proliferation. Oncogene 2004;23:5748–5758.

49. Takahashi K, Tanabe K, Ohnuki M, et al. Induction of pluripotent stem cells from adult human fibroblasts by defined factors. Cell 2007;131:861–872.
50. Chaudry MA, Sales K, Ruf P, et al. EpCAM an immunotherapeutic target for gastrointestinal malignancy: current experience and future challenges. Br J Cancer 2007;96:1013–1019.
51. Nagrath S, Sequist LV, Maheswaran S, et al. Isolation of rare circulating tumour cells in cancer patients by microchip technology. Nature 2007;450:1235–1241.

Received March 9, 2008. Accepted December 1, 2008.

Reprint requests

Address requests for reprints to: Xin Wei Wang, PhD, Liver Carcinogenesis Section, Laboratory of Human Carcinogenesis, Center for Cancer Research, National Cancer Institute, 37 Convent Drive, Building 37, Room 3044A, MSC 4258, Bethesda, Maryland 20892-4258. e-mail: xw3u@nih.gov; fax: (301) 496-0497.

Acknowledgments

Microarray data are available publicly at http://www.ncbi.nlm.nih.gov/geo/ (accession number: GSE5975).

The authors thank Drs Curtis Harris and Sharon Pine for critical readings of the manuscript; Ms Barbara Taylor and Dr Susan Garfield for technical assistance; Drs Ali Brivanlou (Rockefeller University), Steve Strom (University of Pittsburgh), and Bert Vogelstein (Johns Hopkins University) for generously providing their research materials.

Conflicts of interest

The authors disclose no conflicts.

Funding

The authors disclose the following: This work was supported in part by the Intramural Research Program of the Center for Cancer Research, the US National Cancer Institute. Dr Yang, Dr HY Wang, Dr Jia, Dr Ye, Dr Qin, and Dr Tang were supported by research grants from the China National Natural Science Foundation for Distinguished Young Scholars (30325041) and the China National "863" R&D High-Tech Key Project (2002BA711A02-4). Dr Reid was supported by a sponsored research grant from Vesta Therapeutics (Research Triangle Park, NC), National Institutes of Health grants (RO1 AA014243 and RO1 IP30-DK065933), and a US Department of Energy grant (DE-FG02-02ER-63477). Sponsors had no role in the study design, data collection, analysis, and interpretation. Dr Yamashita, Dr Ji, Dr Budhu, Dr Forgues, Dr Yang, Dr Wang, Dr Jia, Dr Ye, Dr Wauthier, Dr Minato, Dr Honda, Dr Kaneko, and Dr Wang disclose no conflicts.

Supplementary Materials and Methods

FACS and MACS Analyses

Cultured cells were trypsinized, washed, and resuspended in Hank's balanced salt solutions (Lonza, Basel, Switzerland) supplemented with 1% HEPES and 2% fetal bovine serum. Cells then were incubated with FITC-conjugated anti-EpCAM monoclonal antibody Clone Ber-EP4 (DAKO, Carpinteria, CA) on ice for 30 minutes, and $EpCAM^+$ and $EpCAM^-$ cells were isolated by a BD FACSAria cell sorting system (BD Biosciences). For magnetic separation, cells were labeled 24 hours after enzymatic dissociation with primary EpCAM antibody (mouse IgG1; Dako), subsequently magnetically labeled with rat anti-mouse IgG1 Microbeads, and separated on a MACS LS column (Miltenyi Biotec, Inc, Auburn, CA). All the procedures were performed according to the manufacturer's instructions. The purity of sorted cells was evaluated by FACS. Fixed cells also were analyzed by FACS using a FACSCalibur (BD Biosciences). Anti-EpCAM antibody VU-1D9, anti-CD133/2 clone 293C3 (Miltenyi Biotec Inc), and anti-CD90 clone 5E10 (StemCell Technologies Inc, Vancouver, British Columbia, Canada) were used to detect $EpCAM^+$, $CD133^+$, or $CD90^+$ cells. Intracellular AFP levels were examined by a BD Cytofix/Cytoperm Fixation/Permeabilization Kit (San Jose, CA) and anti-AFP rabbit polyclonal antibody (DAKO).

Quantitative Reverse Transcription–Polymerase Chain Reaction and IHC Analyses

Total RNA was extracted using TRIzol (Invitrogen) according to the manufacturer's instructions. The expression of selected genes was determined in triplicate using the Applied Biosystems 7500 Sequence Detection System (Applied Biosystems, Foster City, CA) as previously described.[1] Genes expressed in embryonic stem cells were determined in quadruplicate using TaqMan Human Stem Cell Pluripotency Array (Applied Biosystems). IHC analyses with specific antibodies were performed essentially as previously described.[1] Confocal fluorescence microscopic analysis was performed essentially as previously described.[2]

References

1. Yamashita T, Forgues M, Wang W, et al. EpCAM and alpha-fetoprotein expression defines novel prognostic subtypes of hepatocellular carcinoma. Cancer Res 2008;68:1451–1461.
2. Wang W, Budhu A, Forgues M, et al. Temporal and spatial control of nucleophosmin by the Ran-Crm1 complex in centrosome duplication. Nat Cell Biol 2005;7:823–830.

Supplemetary Table 1. Clinicopathologic Characteristics of HpSC-HCC and MH-HCC Cases Used for Oligonucleotide Microarray Analyses

Parameters	HpSC-HCC (n = 60)	MH-HCC (n = 96)	*P* value[a]
Mean age, *y* (SD)	46.0 ± 10.7	52.9 ± 10.5	.0004
Sex: male/female	50/10	87/9	.18
Cirrhosis: yes/no/no data	56/4	88/7/1	.72
Median AFP level, *ng/mL* (25%–75%)	1706 (865–5915)	11.8 (4.0–48.6)	<.0001
Histologic grade[b]			
I–II	14	41	
II–III	44	48	
III–IV	2	5	
No data	0	2	.031
Mean tumor size, *cm* (SD)	5.1 ± 3.0	4.4 ± 3.0	.088
Multinodular: yes/no	16/44	15/81	.09
Portal vein invasion, yes/no[c]	11/49	9/87	.10
TNM classification			
I	24	46	
II	22	42	
III	14	8	.03
Virus status: HBV/HBV + HCV/unknown	56/4/0	95/0/1	.43

[a]Mann–Whitney *U* test or χ^2 test.
[b]Edmondson–Steiner.
[c]Macroscopic portal vein invasion.

Supplementary Table 2. Clinicopathologic Characteristics of HpSC-HCC and MH-HCC Cases Used for IHC

Parameters	HpSC-HCC (n = 24)	MH-HCC (n = 55)	*P* value[a]
Mean age, *y* (SD)	46.4 ± 9.4	58.4 ± 11.9	< .0001
Sex: male/female	20/4	48/7	.64
Cirrhosis: yes/no	23/1	46/9	.14
Median AFP level, *ng/mL* (25%–75%)	1620 (887–3166)	12 (9.3–219)	< .0001
Histologic grade[b]			
I–II	12	32	
II–III	8	21	
III–IV	4	2	.13
Mean tumor size, *cm* (SD)	7.1 ± 3.6	5.2 ± 3.6	.014
Multinodular: yes/no	4/20	16/39	.24
Portal vein invasion: yes/no[c]	12/12	12/43	.012
TNM classification			
I	4	19	
II	8	20	
III	12	16	.14
Virus status: HBV/HCV/unknown	21/2/1	32/21/2	.026

[a]Mann–Whitney *U* test or χ^2 test.
[b]Edmondson–Steiner.
[c]Macroscopic portal vein invasion.

Supplementary Table 3. Top 10 List of Canonical Pathways Activated in HpSC-HCC From Ingenuity Pathway Analysis

Pathways	Genes included in cluster A
Axonal guidance signaling	
Up	ROBO2, ARPC5L (includes EG:81873), SEMA4G, PDGFRB, PLCB1, PRKCD, FGFR3, FZD5, MERTK, DDR1, LINGO1, SEMA3C
Down	PIK3C3, IGF1, PIK3C2G, MAP2K2, ARHGEF15
Transforming growth factor-β signaling	
Up	PDGFRB, FGFR3, MERTK, UBD, DDR1, SMAD5
Down	MAP2K2, HNF4A
Integrin signaling	
Up	ARPC5L (includes EG:81873), PDGFRB, FGFR3, GRB7, MERTK, ITGB5, DDR1, DDEF1
Down	PIK3C3, MYLK, PIK3C2G, MAP2K2
Apoptosis signaling	
Up	PDGFRB, BAK1, CYCS, FGFR3, MERTK, DDR1
Down	MAP3K5, MAP2K2
G2/M DNA damage checkpoint regulation	
Up	YWHAZ, CCNB2, UBD, WEE1
Down	CDKN2A, GADD45A
ERK/MAPK signaling	
Up	ELF3, PDGFRB, YWHAZ, PRKCD, FGFR3, MERTK, DDR1
Down	PIK3C3, DUSP1, PIK3C2G, ESR1, MAP2K2
Wnt/β-catenin signaling	
Up	DKK1, SOX9, FZD5, UBD, TCF7L2, CSNK1E
Down	CDKN2A, RARG
PI3K/AKT signaling	
Up	PDGFRB, YWHAZ, FGFR3, MERTK, DDR1
Down	MAP3K5, MAP2K2, GYS2
Amyloid processing	
Up	BACE2, CSNK1E, MAPK13
Down	
Leukocyte extravasation signaling	
Up	PRKCD, CLDN4, CLDN1, MMP11, MAPK13
Down	PIK3C3, CLDN2, PIK3C2G, MAP2K2

NOTE. The top 10 pathways were selected based on the significance for the enrichment of the genes with a particular canonical signaling pathway determined by the one-sided Fisher exact test ($P < .01$).

Supplementary Table 4. Top 10 List of Canonical Pathways Activated in MH-HCC From Ingenuity Pathway Analysis

Pathways	Genes included in cluster B
Lipopolysaccharide/interleukin-1–mediated inhibition of RXR function	
Up	SULT1C2, ACSL4, ACSL3, FABP5, GSTP1
Down	NR1I2, NR1I3, CYP7A1, ALDH1L1, ABCB1, SLC10A1, SLC27A2, CD14, GSTM1, ALDH6A1, GSTM4, ACSL5, CES2 (includes EG:8824), FMO3, SULT2A1 (includes EG:6822), GSTA1, CYP2C8, LC27A5, CYP3A7, ABCG5, ALDH8A1, APOC4 (includes EG:346), CYP3A4, ACSL1, ABCB11, FMO4, MAOA
Xenobiotic metabolism signaling	
Up	SULT1C2, PRKCD, GSTP1, MAPK13
Down	NR1I2, NR1I3, ALDH1L1, ABCB1, UGT2B15, MAP2K2, UGT2B7, PPARGC1A, GSTM1, PIK3C3, ALDH6A1, GSTM4, CES2 (includes EG:8824), MAP3K5, FMO3, PIK3C2G, SULT2A1 (includesEG:6822), CYP1A2, GSTA1, CYP2C8, CYP3A7, NQO2, ALDH8A1, CYP3A4, CES1 (includes EG:1066), FMO4, MAOA
Hepatic cholestasis	
Up	ADCY3, PRKCD
Down	CD14, ABCG5, NR1I2, CYP7A1, CYP7B, CYP8B1, ABCB1, ESR1, SLC10A1, ABCB11, ABCB4, HNF4A
Aryl hydrocarbon receptor signaling	
Up	GSTP1
Down	CDKN2A, NQO2, GSTM1, ALDH8A1, ALDH6A1, ALDH1L1, GSTM4, ESR1, CYP1A2, GSTA1, RARG
NRF2-mediated oxidative stress response	
Up	DNAJA4, PRKCD, GSTP1
Down	NQO2, GSTM1, AOX1, PIK3C3, GSTM4, MAP3K5, SOD1, PIK3C2G, MAP2K2, FKBP5, GSTA1
Complement system	
Up	
Down	C8A, C1R, MASP1, C6, C8B, MASP2
Coagulation system	
Up	
Down	SERPINC1, KLKB1, F9, KNG1 (includes EG:3827), F11
Acute-phase response signaling	
Up	MAPK13
Down	APCS, RBP5, C1R, MAP3K5, HRG, MAP2K2, KLKB1, SAA4
p53 signaling	
Up	THBS1
Down	CDKN2A, PIK3C3, SNAI2, GADD45A, PIK3C2G, GADD45B
LXR/RXR activation	
Up	HMGCR
Down	CD14, ABCG5, APOA5, CYP7A1, APOC4 (includes EG:346)

LXR/RXR, liver X receptor/retinoid X receptor; NRF2, NF-E2-related factor 2.
NOTE. The top 10 pathways were selected based on the significance for the enrichment of the genes with a particular canonical signaling pathway determined by the one-sided Fisher exact test ($P < .01$).

Author's Choice

THE JOURNAL OF BIOLOGICAL CHEMISTRY VOL. 284, NO. 22, pp. 14809–14818, May 29, 2009

Palmitate Induces Insulin Resistance in H4IIEC3 Hepatocytes through Reactive Oxygen Species Produced by Mitochondria*[S]

Received for publication, March 5, 2009 Published, JBC Papers in Press, March 30, 2009, DOI 10.1074/jbc.M901488200

Seiji Nakamura[‡], Toshinari Takamura[‡1], Naoto Matsuzawa-Nagata[§], Hiroaki Takayama[‡], Hirofumi Misu[‡], Hiroyo Noda[‡], Satoko Nabemoto[‡], Seiichiro Kurita[‡], Tsuguhito Ota[‡], Hitoshi Ando[‡], Ken-ichi Miyamoto[§], and Shuichi Kaneko[‡]

From the [‡]Department of Disease Control and Homeostasis, Kanazawa University Graduate School of Medical Science, and the [§]Department of Medicinal Informatics, Kanazawa University Hospital, 13-1 Takara-machi, Kanazawa 920-8641, Japan

Visceral adiposity in obesity causes excessive free fatty acid (FFA) flux into the liver via the portal vein and may cause fatty liver disease and hepatic insulin resistance. However, because animal models of insulin resistance induced by lipid infusion or a high fat diet are complex and may be accompanied by alterations not restricted to the liver, it is difficult to determine the contribution of FFAs to hepatic insulin resistance. Therefore, we treated H4IIEC3 cells, a rat hepatocyte cell line, with a monounsaturated fatty acid (oleate) and a saturated fatty acid (palmitate) to investigate the direct and initial effects of FFAs on hepatocytes. We show that palmitate, but not oleate, inhibited insulin-stimulated tyrosine phosphorylation of insulin receptor substrate 2 and serine phosphorylation of Akt, through c-Jun NH_2-terminal kinase (JNK) activation. Among the well established stimuli for JNK activation, reactive oxygen species (ROS) played a causal role in palmitate-induced JNK activation. In addition, etomoxir, an inhibitor of carnitine palmitoyltransferase-1, which is the rate-limiting enzyme in mitochondrial fatty acid β-oxidation, as well as inhibitors of the mitochondrial respiratory chain complex (thenoyltrifluoroacetone and carbonyl cyanide *m*-chlorophenylhydrazone) decreased palmitate-induced ROS production. Together, our findings in hepatocytes indicate that palmitate inhibited insulin signal transduction through JNK activation and that accelerated β-oxidation of palmitate caused excess electron flux in the mitochondrial respiratory chain, resulting in increased ROS generation. Thus, mitochondria-derived ROS induced by palmitate may be major contributors to JNK activation and cellular insulin resistance.

Insulin is the major hormone that inhibits gluconeogenesis in the liver. Visceral adiposity in obesity causes hepatic steatosis and insulin resistance. In an insulin-resistant state, impaired insulin action allows enhancement of glucose production in the liver, resulting in systemic hyperglycemia (1) and contributing to the development of type 2 diabetes. In addition, we have demonstrated experimentally that insulin resistance accelerated the pathology of steatohepatitis in genetically obese diabetic OLETF rats (2). In contrast, lipid-induced oxidative stress caused steatohepatitis and hepatic insulin resistance in mice (3). In fact, steatosis of the liver is an independent predictor of insulin resistance in patients with nonalcoholic fatty liver disease (4).

It remains unclear whether hepatic steatosis causally contributes to insulin resistance or whether it is merely a resulting pathology. Excessive dietary free fatty acid (FFA)[2] flux into the liver via the portal vein may cause fatty liver disease and hepatic insulin resistance. Indeed, elevated plasma FFA concentrations correlate with obesity and decreased target tissue insulin sensitivity (5).

Experimentally, lipid infusion or a high fat diet that increases circulating FFA levels promotes insulin resistance in the liver. Candidate events linking FFA to insulin resistance *in vivo* are the up-regulation of SREBP-1c (6), inflammation caused by activation of c-Jun amino-terminal kinase (JNK) (7) or IKKβ (8), endoplasmic reticulum (ER) stress (9), ceramide (10, 11), and TRB3 (12).

However, which event is the direct and initial target of FFA in the liver is unclear. Insulin resistance induced by lipid infusion or a high fat diet is complex and may be accompanied by alterations not restricted to the liver, making it difficult to determine the contribution of FFAs to hepatic insulin resistance. For example, hyperinsulinemia and hyperglycemia secondary to the initial event also may contribute to the development of diet-induced insulin resistance *in vivo* (6).

To address the early event(s) triggering the development of high fat diet- or obesity-induced insulin resistance, we investigated the molecular mechanism(s) underlying the direct action of FFA on hepatocytes to cause insulin resistance *in vitro*, using the rat hepatocyte cell line H4IIEC3. We found that mitochondria-derived reactive oxygen species (ROS) were a cause of palmitate-induced insulin resistance in hepatocytes.

* This work was supported by grants-in-aid from the Ministry of Education, Culture, Sports, Science, and Technology of Japan.
Author's Choice—Final version full access.
[S] The on-line version of this article (available at http://www.jbc.org) contains supplemental Figs. 1–8.
[1] To whom correspondence should be addressed. Tel.: 81-76-265-2233; Fax: 81-76-234-4250; E-mail: ttakamura@m-kanazawa.jp.

[2] The abbreviations used are: FFA, free fatty acid; IRS, insulin receptor substrate; JNK, c-Jun NH_2-terminal kinase; ER, endoplasmic reticulum; ROS, reactive oxygen species; NAC, *N*-acetyl-L-cysteine; H2DCFDA, 2′,7′-dichlorofluorescin diacetate; OXPHOS, oxidative phosphorylation; PVDF, polyvinylidene difluoride.

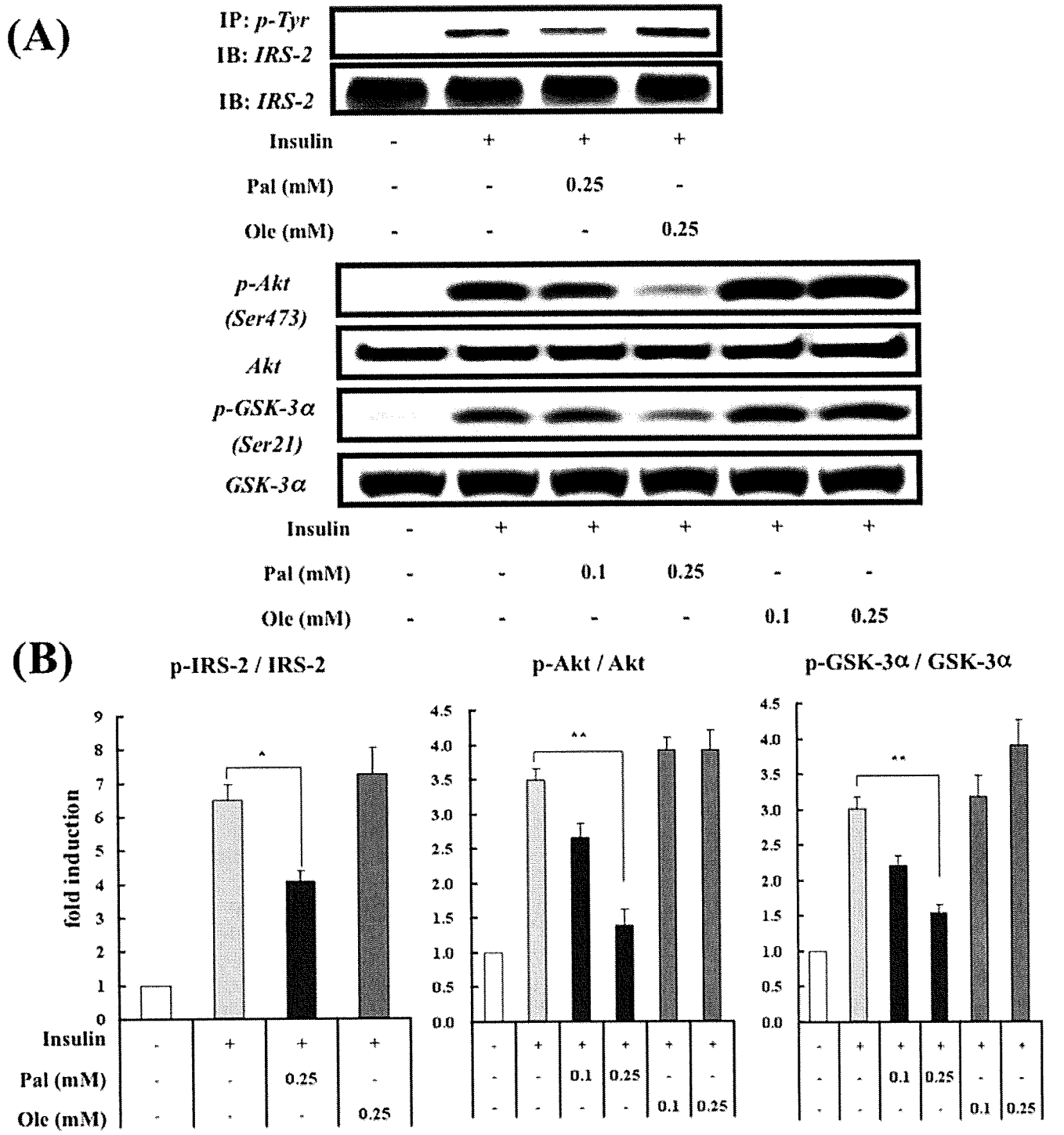

FIGURE 1. **Effects of palmitate and oleate on insulin-stimulated tyrosine phosphorylation of IRS-2 and serine phosphorylation of Akt and GSK-3 in H4IIEC3 hepatocytes.** *A*, H4IIEC3 cells were incubated in the presence or absence of palmitate (*Pal*) or oleate (*Ole*) for 16 h prior to stimulation with insulin (1 ng/ml, 15 min). Total cell lysates were resolved by SDS-PAGE, transferred to a PVDF membrane, and immunoblotted (*IB*) with the indicated antibodies. Total cell lysates were subjected to immunoprecipitation (*IP*) with phosphotyrosine antibody prior to SDS-PAGE to examine tyrosine phosphorylation of IRS-2. Detection was by enhanced chemiluminescence. Representative blots are shown. *B*, the values from densitometry of three (p-IRS-2), eight (p-Akt), or five (p-GSK-3α) independent experiments were normalized to the level of total IRS-2, Akt, or GSK-3α protein, respectively, and expressed as the mean -fold increase over control ± S.E. *, $p < 0.05$ *versus* insulin treatment alone. **, $p < 0.01$ *versus* insulin treatment alone.

EXPERIMENTAL PROCEDURES

Materials—The antibody against IRS-2 was purchased from Upstate Biotechnology, Inc. (Lake Placid, NY). Antibodies against phosphotyrosine, Akt, phospho-Akt (Ser^{473}), stress-activated protein kinase/JNK, phospho-stress-activated protein kinase/JNK (Thr^{183}/Tyr^{185}), and phospho-GSK (glycogen synthase kinase)-3 ($Ser^{21/9}$) were purchased from Cell Signaling Technology (Beverly, MA). Antibodies against GSK-3 and phospho-c-Jun were from Santa Cruz Biotechnology, Inc. (Santa Cruz, CA). Insulin from porcine pancreas, sodium

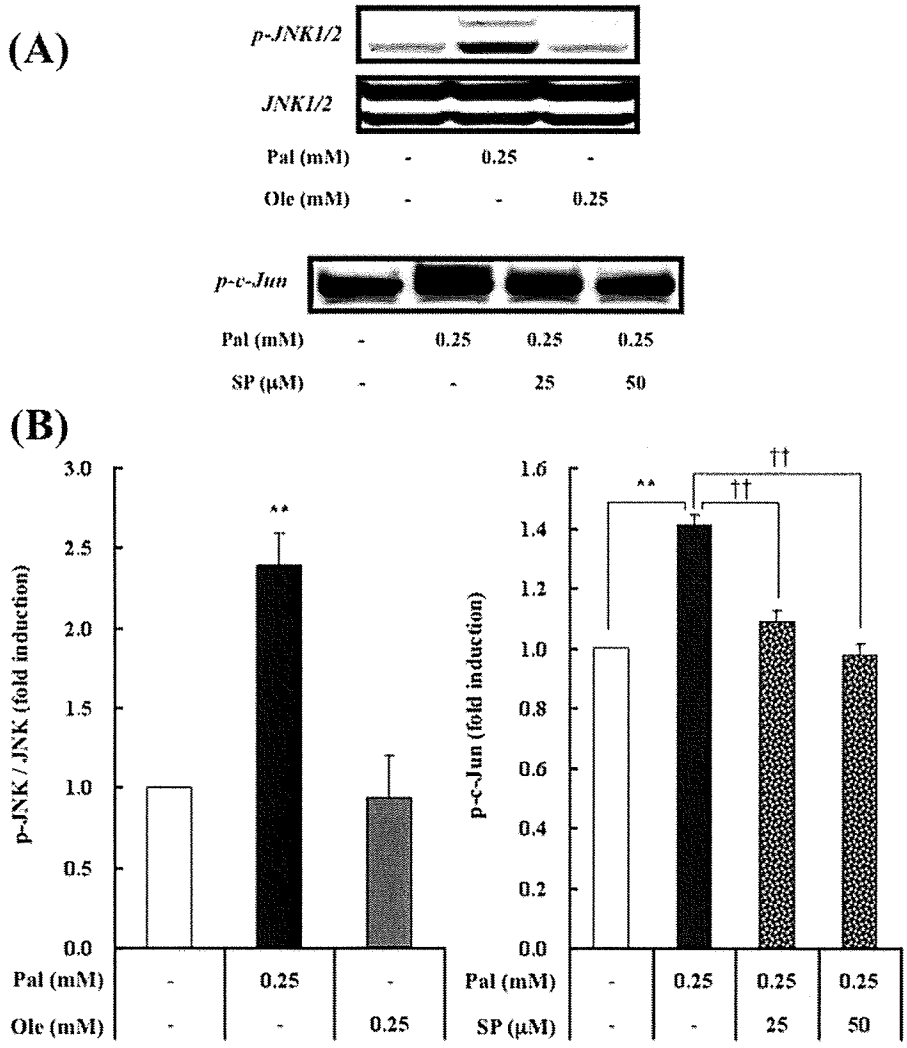

FIGURE 2. **Effects of palmitate and oleate on JNK activation in H4IIEC3 hepatocytes.** *A*, H4IIEC3 cells were incubated in the presence or absence of FFAs (palmitate (*Pal*) or oleate (*Ole*)) and the JNK inhibitor SP600125 (*SP*) for 16 h. Total cell lysates were resolved by SDS-PAGE, transferred to a PVDF membrane, and immunoblotted with the indicated antibodies. Detection was by enhanced chemiluminescence. Representative blots are shown. *B*, the values from densitometry of four (p-JNK) independent experiments were normalized to the level of total JNK (p-c-Jun was not normalized; $n = 4$) and expressed as the mean -fold increase over control ± S.E. **, $p < 0.01$ *versus* control. ††, $p < 0.01$ *versus* palmitate treatment.

palmitate, sodium oleate, myriocin, *N*-acetyl-L-cysteine, rotenone, thenoyltrifluoroacetone, cyanide *m*-chlorophenylhydrazone, oxypurinol, etomoxir, and tunicamycin was obtained from Sigma. SP600125 and apocynin were from Calbiochem. DL-α-tocopherol and 2′,7′-dichlorofluorescin diacetate (H_2DCFDA) were from Wako (Osaka, Japan).

Cell Culture and Fatty Acid Treatment—Studies were performed in the rat hepatoma cell line H4IIEC3, purchased from the American Type Culture Collection (Manassas, VA). Cells were cultured in Dulbecco's modified Eagle's medium (Invitrogen) supplemented with 10% fetal bovine serum (Invitrogen), penicillin (100 units/ml), and streptomycin (0.1 mg/ml; Invitrogen). The cells were cultured at 37 °C in a humidified atmosphere containing 5% CO_2, with medium changes three times a week. All studies were conducted using 80–90% confluent cells, which were treated with the indicated concentrations of FFAs in the presence of 2% FFA-free bovine serum albumin (Sigma).

Cell Harvest and Western Blot Analysis—H4IIEC3 hepatocytes, grown to 80–90% confluence in 6-well plates, were treated with the indicated reagents for 16 h in Dulbecco's modified Eagle's medium. After treatment, the cells were stimulated with insulin (1 ng/ml) for 15 min. Then the cells were washed with ice-cold phosphate-buffered saline and lysed in buffer containing 20 mM Tris-HCl (pH 7.5), 5 mM EDTA, 1% Nonidet P-40, 2 mM Na_3VO_4, 100 mM NaF, and a protease inhibitor mixture (Sigma). After sonication with a Bioruptor (Cosmo Bio, Tokyo, Japan), the lysates were centrifuged to remove insoluble materials. The supernatants (10 μg/lane) were separated by SDS-PAGE and transferred onto polyvinylidene difluoride membranes (Millipore, Billerica, MA). For detection of phosphotyrosine insulin receptor and phosphotyrosine IRS-2, the supernatants (400 μg of protein) were immunoprecipitated with a phosphotyrosine antibody and protein G beads for 2 h at 4 °C before SDS-PAGE. The membranes were blocked in a buffer containing 5% nonfat milk, 50 mM Tris (pH 7.6), 150 mM NaCl, and 0.1% Tween 20 (TBS-T) for 1 h at room temperature. They were then incubated with specific primary antibodies and subsequently with horseradish peroxidase-linked secondary antibodies. Signals were detected with a chemiluminescence detection system (ECL Plus Western blotting detection reagents; GE Healthcare). Densitometric analysis was conducted directly on the blotted membrane, using a CCD camera system (LAS-3000 Mini; Fujifilm, Tokyo, Japan) and Scion Image software.

Quantitative Real Time PCR—Total RNA was extracted from cultured H4IIEC3 hepatocytes using an RNeasy mini kit (Qiagen, Germantown, MD), according to the manufacturer's protocol. The cDNA was synthesized from total RNA (100 ng) using random hexamer primers, N_6, and a high capacity cDNA reverse transcription kit (Applied Biosystems, Foster City, CA). Quantitative real time PCR was performed with an ABI Prism 7900HT (Applied Biosystems). The set of specific primers and TaqMan probes in the present study was obtained from Applied Biosystems. The PCR conditions were one cycle at 50 °C for 2 min and 95 °C for 10 min, followed by 40 cycles at 95 °C for 15 s and 60 °C for 1 min.

Analysis of XBP-1 (X-box-binding Protein-1) mRNA Splicing—Total RNA was extracted from H4IIEC3 hepatocytes, and

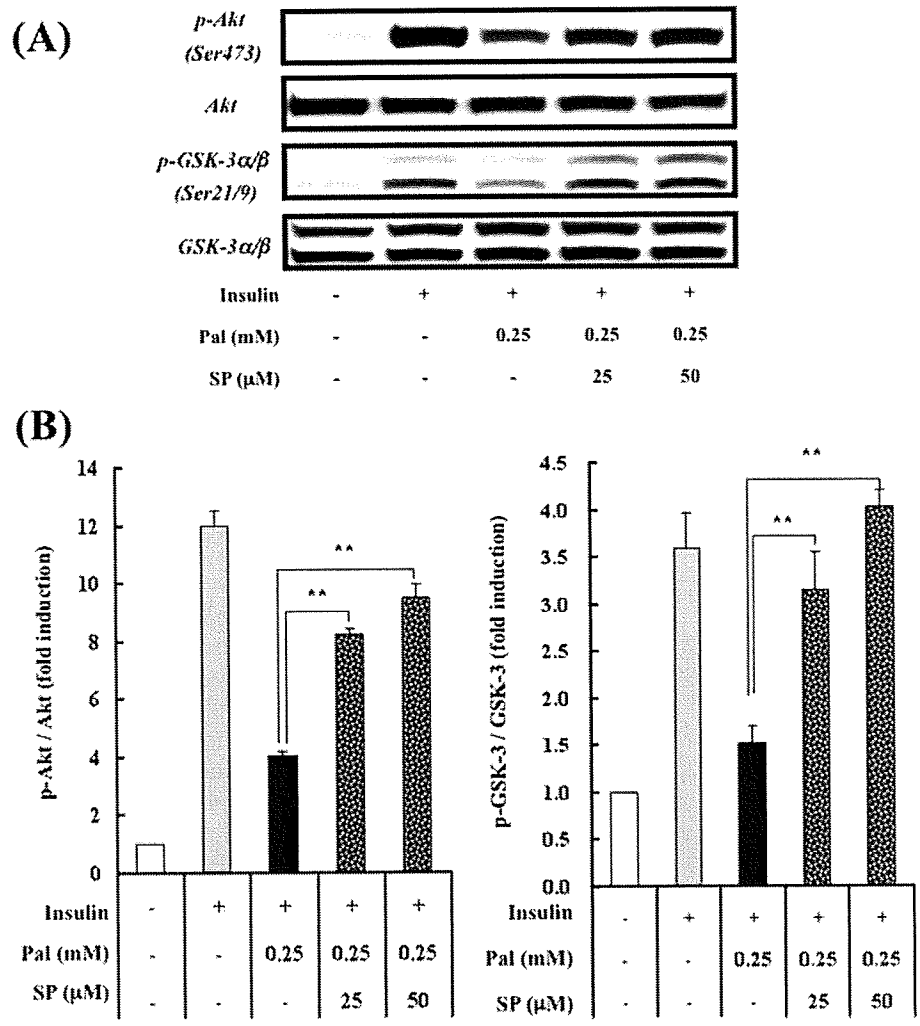

FIGURE 3. **Effect of a JNK inhibitor on palmitate-induced alterations in insulin-stimulated phosphorylation of Akt and GSK-3 in H4IIEC3 hepatocytes.** *A*, H4IIEC3 cells were incubated in the presence or absence of palmitate (*Pal*) and the JNK inhibitor SP600125 (*SP*) for 16 h prior to stimulation with insulin (1 ng/ml, 15 min). Total cell lysates were resolved by SDS-PAGE, transferred to a PVDF membrane, and immunoblotted with the indicated antibodies. Detection was enhanced by chemiluminescence. Representative blots are shown. *B*, the values from densitometry of four (p-Akt or p-GSK-3) independent experiments were normalized to the level of total Akt or GSK-3 protein, respectively, and expressed as the mean -fold increase over control ± S.E. **, $p <$ 0.01 *versus* palmitate treatment.

cDNA was synthesized as described above. The cDNA was amplified with a pair of primers (reverse 5′-CCA TGG GAA GAT GTT CTG GG-3′ and forward 5′-ACA CGC TTG GGG ATG AAT GC-3′) corresponding to the rat XBP-1 cDNA. The PCR conditions were initial denaturation at 94 °C for 3 min, followed by 30 cycles of amplification (94 °C for 30 s, 58 °C for 30 s, 72 °C for 30 s) and a final extension at 72 °C for 3 min. The PCR products were separated by 2.5% agarose gel electrophoresis.

Measurement of Intracellular ROS—The intracellular formation of ROS was detected using the fluorescent probe H_2DCFDA, according to a published method (13). Briefly, H4IIEC3 hepatocytes, grown to 70 – 80% confluence in 96-well plates, were treated with the indicated reagents in Dulbecco's modified Eagle's medium for 8 h. After treatment, the cells were washed with phosphate-buffered saline, loaded with 10 μM H_2DCFDA, and incubated for 30 min at 37 °C. The fluorescence was analyzed using a plate reader (Fluoroskan Ascent FL, ThermoLab Systems, Franklin, MA).

Measurement of Protein Carbonyls—The cellular concentration of proteins containing carbonyl groups (those that react with 2,4-dinitrophenylhydrazine to form the corresponding hydrazone) was determined spectrophotometrically using a protein carbonyl assay kit (Cayman Chemical, Ann Arbor, MI) according to the manufacturer's instructions and as described previously (14).

Statistical Analysis—All values are given as means ± S.E. Differences between two groups were assessed using unpaired, two-tailed *t* tests. Data involving more than two groups were assessed by one-way analysis of variance. All calculations were performed with SPSS (version 12.0 for Windows; SPSS, Chicago, IL).

RESULTS

Palmitate Inhibited Insulin Receptor-mediated Signaling—Two long chain fatty acids were chosen for the study: palmitate, a C16:0 saturated fatty acid, and oleate, a C18:1 monounsaturated fatty acid. To examine whether FFAs impaired insulin signal transduction in H4IIEC3 hepatocytes, we assessed the effect of FFAs on insulin-stimulated tyrosine phosphorylation of IRS-2 and serine phosphorylation of Akt and GSK-3α (Fig. 1). Incubation with 0.25 mM palmitate inhibited insulin-stimulated tyrosine phosphorylation of IRS-2 by 40% in H4IIEC3 cells. Downstream of IRS-2, insulin-stimulated serine phosphorylation of Akt and GSK-3α were also inhibited by 0.25 mM palmitate treatment, by 80 and 70%, respectively, indicating an insulin-resistant state. However, the protein levels of total IRS-2, Akt, and GSK-3 were unaffected by palmitate. Furthermore, we confirmed that palmitate, but not oleate, impaired insulin-stimulated Akt serine phosphorylation in the human hepatoma cell line HepG2 (supplemental Fig. 1).

JNK Activation by Palmitate Contributes to Palmitate-induced Insulin Resistance—JNK, a stress-activated protein kinase, has been reported to phosphorylate IRS-1 and -2 at serine residues (15, 16). Serine phosphorylation of IRSs impairs IRS tyrosine phosphorylation, leading to a reduction in insulin receptor-mediated signaling. Many studies have verified the role of JNK in fat-induced insulin resistance in several experimental systems (7, 17, 18). Thus, we next examined the effect of FFAs on JNK activation and its involvement in insulin signaling. Palmitate, but not oleate, dramatically increased phosphoryla-

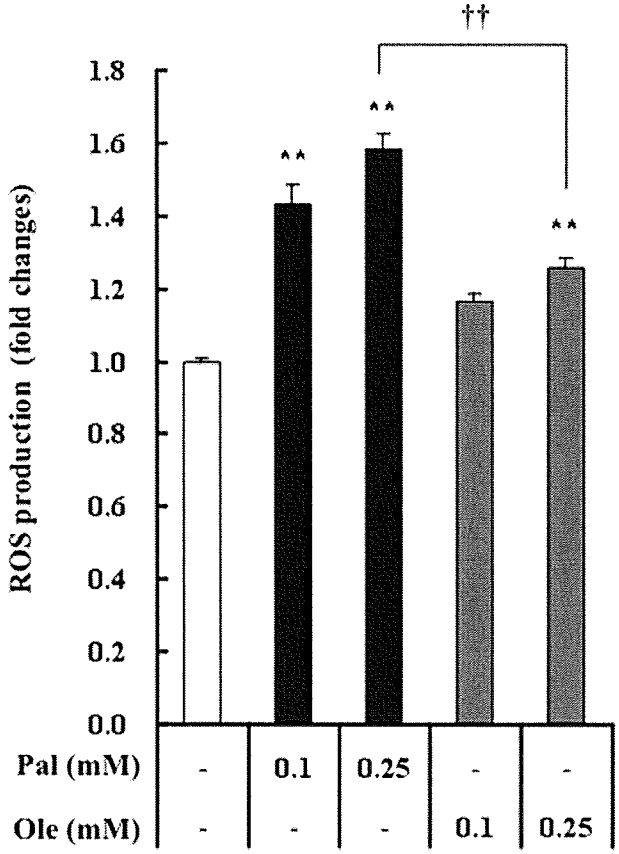

FIGURE 4. **Effect of palmitate on oxidative stress in H4IIEC3 hepatocytes.** H4IIEC3 cells were incubated in the presence or absence of palmitate (*Pal*) or oleate (*Ole*) for 8 h. Intracellular ROS production was quantified using the fluorescent probe H_2DCFDA. The values are expressed as mean -fold increase over control ± S.E. ($n = 4$). **, $p < 0.01$ *versus* control. ††, $p < 0.01$ *versus* 0.25 mM palmitate treatment.

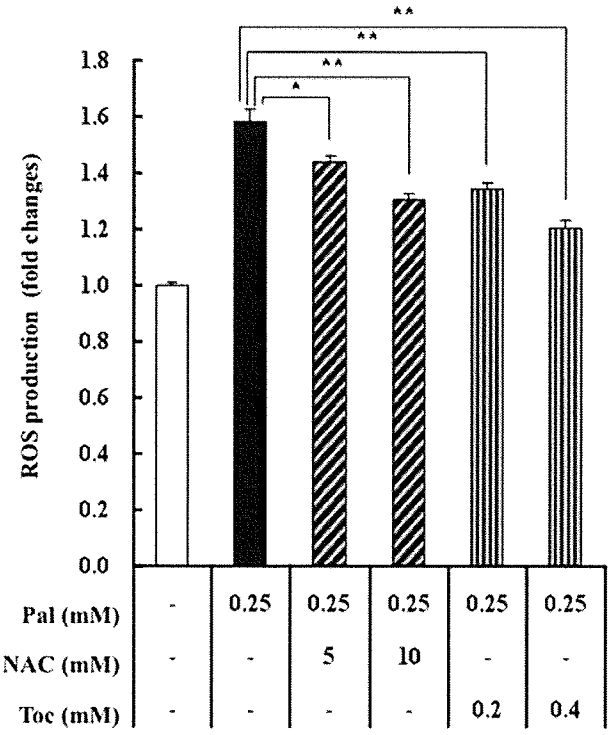

FIGURE 5. **Effects of antioxidants on palmitate-induced intracellular ROS production in H4IIEC3 hepatocytes.** H4IIEC3 cells were incubated in the presence or absence of palmitate (*Pal*) and antioxidants for 8 h. Intracellular ROS production was quantified using the fluorescent probe H_2DCFDA. The values are expressed as mean -fold increase over control ± S.E. ($n = 4$). *, $p < 0.05$ *versus* palmitate treatment alone. **, $p < 0.01$ *versus* palmitate treatment alone. *NAC*, *N*-acetyl-L-cysteine; *Toc*, α-tocopherol.

ted JNK and c-Jun (Fig. 2). A potent and selective inhibitor of JNK, SP600125 (19), reversed the palmitate-induced phosphorylation of c-Jun (Fig. 2), suggesting that palmitate activated JNK. To test whether palmitate-induced JNK activation mediated cellular insulin resistance, we inhibited the JNK pathway with SP600125. SP600125 dose-dependently improved insulin-stimulated serine phosphorylation of Akt and GSK-3 in H4IIEC3 hepatocytes exposed to palmitate (Fig. 3). These results suggest that JNK activation by palmitate contributed to palmitate-induced insulin resistance.

Pathways for SREBP-1c and ER Stress Are Not Involved in Palmitate-induced JNK Activation and Insulin Resistance in H4IIEC3 Hepatocytes—The SREBP-1c pathway has been reported to play a role in diet-induced insulin resistance *in vivo*. Ide *et al.* (6) found that high sucrose diet-induced hyperglycemia and hyperinsulinemia up-regulated hepatic expression of SREBP-1c, leading to down-regulation of IRS-2 at the transcriptional level. However, in the present study, palmitate dramatically down-regulated the expression of SREBP-1c in H4IIEC3 hepatocytes (supplemental Fig. 2). Consistent with this, the mRNA (supplemental Fig. 2) and protein (Fig. 1) levels of IRS-2 were unaffected by palmitate. Thus, palmitate itself did not appear to cause insulin resistance in hepatocytes via the SREBP-1c pathway.

ER stress is induced in insulin-resistant states, such as obesity and type 2 diabetes, and in turn, this stress has been shown to lead to the inhibition of insulin signaling, through overactivation of JNK (9). Since excessive FFAs have been shown to trigger ER stress in pancreatic β-cells (20), we examined whether palmitate caused ER stress in H4IIEC3 hepatocytes. ER stress induces the spliced form of XBP-1 (XBP-1s), which up-regulates the transcription of molecular chaperones, including GRP78 (78-kDa glucose-regulated/binding immunoglobulin protein) (21). Palmitate at 0.25 mM did not alter the expression level of GRP78 mRNA or the splicing pattern of XBP-1, unlike tunicamycin, an agent commonly used to induce ER stress (supplemental Fig. 3). Next, we compared the impact of palmitate and tunicamycin on insulin-stimulated signal transduction and JNK activation (supplemental Fig. 4). The inhibitory effect of tunicamycin on insulin-stimulated serine phosphorylation of Akt was mild and not significant compared with that of palmitate. Additionally, the increment in phosphorylated JNK by tunicamycin was lower and not significant compared with that of palmitate. These results suggest that ER stress played a minor role in palmitate-induced JNK activation and cellular insulin resistance in H4IIEC3 hepatocytes.

Palmitate Induces ROS Production—In addition to ER stress, increased cellular ROS levels are known to stimulate threonine phosphorylation of JNK (22). Indeed, ROS levels are increased in clinical conditions associated with insulin resistance, such as sepsis, burn injuries, obesity, and type 2 diabetes (23). Furthermore, FFAs have been reported to generate ROS in various

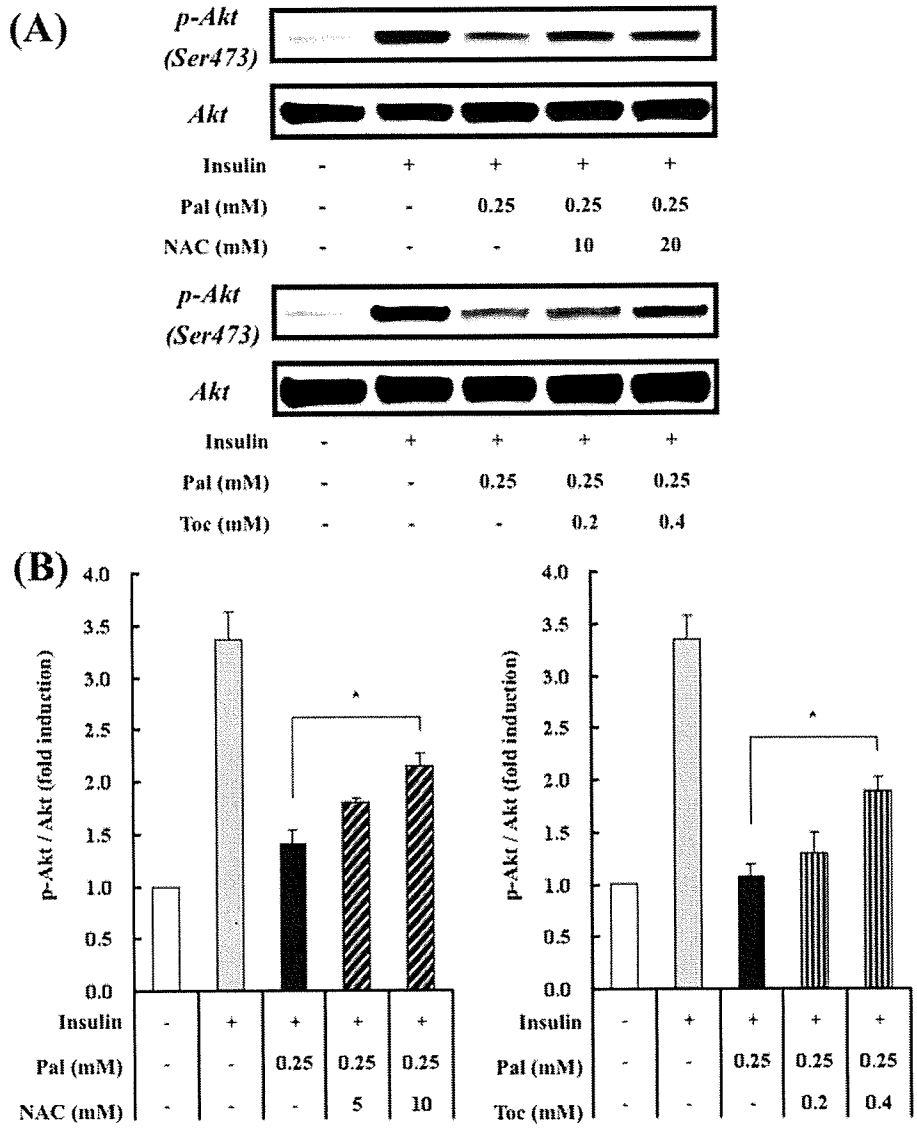

FIGURE 6. **Effects of antioxidants on palmitate-induced alterations in insulin-stimulated serine phosphorylation of Akt in H4IIEC3 hepatocytes.** *A*, H4IIEC3 cells were incubated in the presence or absence of palmitate (*Pal*) and antioxidants for 16 h prior to stimulation with insulin (1 ng/ml, 15 min). Total cell lysates were resolved by SDS-PAGE, transferred to a PVDF membrane, and immunoblotted with the indicated antibodies. Detection was by enhanced chemiluminescence. Representative blots are shown. *B*, the values from densitometry of four (NAC) or five (α-tocopherol) independent experiments were normalized to the level of total Akt protein and expressed as the mean -fold increase over control ± S.E. *, $p < 0.05$ *versus* palmitate treatment. *NAC*, *N*-acetyl-L-cysteine; *Toc*, α-tocopherol.

cells, such as pancreatic islet cells (24), cardiac myocytes (25), and adipocytes (23).

Thus, we hypothesized that palmitate increased intracellular ROS production and thereby activated JNK, leading to the impaired insulin signaling. To evaluate this, H4IIEC3 hepatocytes were incubated with H_2DCFDA, a fluorescent probe, to visualize intracellular ROS, with or without palmitate. H_2DCFDA-associated fluorescence was elevated by 58% after incubation with 0.25 mM palmitate for 8 h, and palmitate induced more ROS production than oleate (Fig. 4). Consistent with this, the amount of protein carbonyls, a marker of oxidative stress, significantly increased in palmitate-treated hepatocytes (4.6 ± 0.5 nmol/mg protein), compared with control cells (3.1 ± 0.4 nmol/mg protein). These results suggest that FFAs, especially palmitate, can cause ROS production and oxidative stress in H4IIEC3 hepatocytes.

Antioxidants Prevent Palmitate-induced Insulin Resistance—We next sought to test whether palmitate-induced ROS overproduction had a causal role in insulin resistance by assessing whether two antioxidant reagents, *N*-acetyl-L-cysteine (NAC) and α-tocopherol, could also act as insulin sensitizers. NAC and α-tocopherol dose-dependently suppressed palmitate-induced intracellular ROS production; NAC at 10 mM and α-tocopherol at 0.4 mM suppressed ROS production by 50 and 60%, respectively (Fig. 5). In parallel with decreased ROS levels, the antioxidants recovered the insulin-stimulated Akt phosphorylation impaired by palmitate; NAC at 10 mM and α-tocopherol at 0.4 mM recovered the phosphorylation by 40 and 35%, respectively (Fig. 6). Furthermore, these antioxidants suppressed palmitate-induced JNK phosphorylation; NAC at 10 mM and α-tocopherol at 0.4 mM suppressed it by 80 and 55%, respectively (Fig. 7). These results suggest that palmitate increased ROS levels in H4IIEC3 hepatocytes and thereby activated JNK, resulting in insulin resistance.

Palmitate Induces ROS Overproduction in Mitochondria—To define the source of ROS induced by palmitate in H4IIEC3 hepatocytes, we examined the cellular pathway involved in ROS production, including NADPH oxidase, xanthine oxidase, and mitochondria-mediated pathways. Palmitate-induced ROS production was markedly suppressed by rotenone, an inhibitor of mitochondrial respiratory chain complex I; thenoyltrifluoroacetone, an inhibitor of mitochondrial respiratory chain complex II; and carbonyl cyanide *m*-chlorophenylhydrazone, an uncoupler of oxidative phosphorylation (Fig. 8). In contrast, ROS production in palmitate-treated H4IIEC3 cells was not suppressed by apocynin, an inhibitor of NADPH oxidase, or oxypurinol, an inhibitor of xanthine oxidase. These results suggest that the mitochondrial respiratory chain is involved in palmitate-induced ROS overproduction in H4IIEC3 hepatocytes.

Palmitate Increases ROS through the Mitochondrial Fatty Acid β-Oxidation Respiratory Chain—FFAs are metabolized in the mitochondrial fatty acid β-oxidation pathway, which sup-

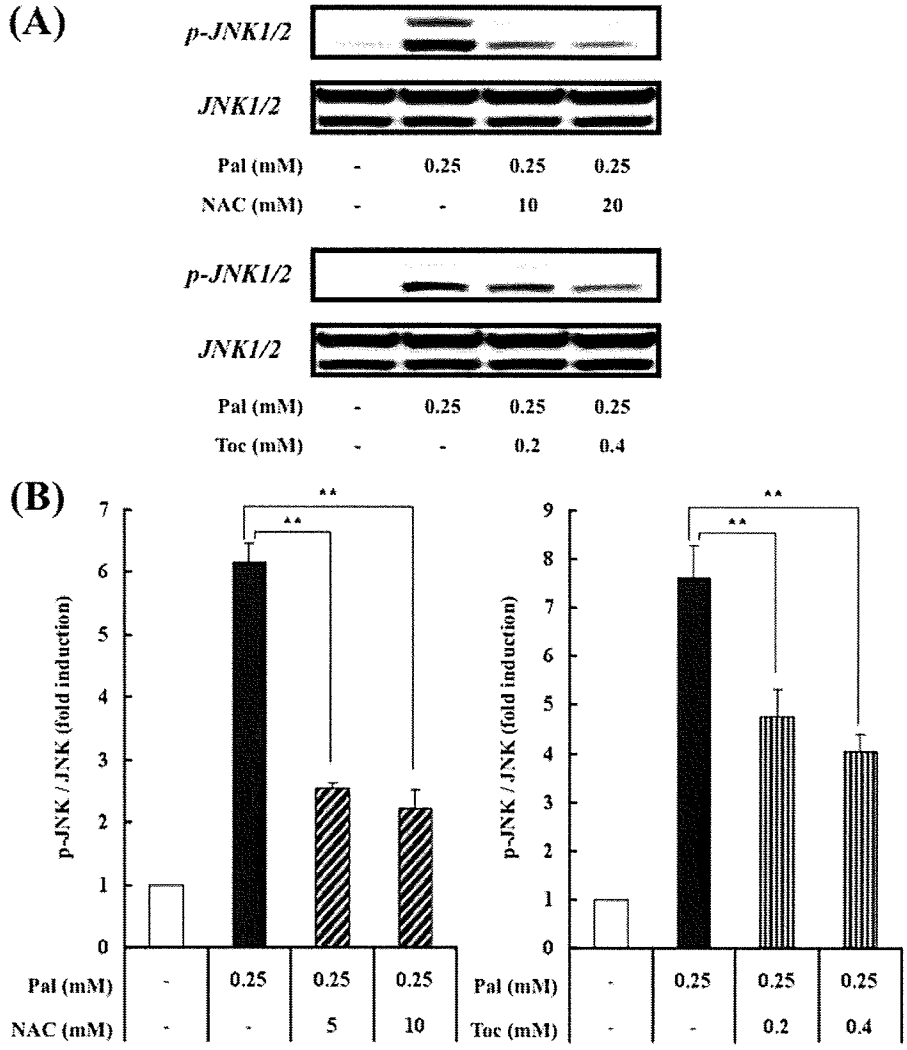

FIGURE 7. **Effects of antioxidants on palmitate-induced JNK activation in H4IIEC3 hepatocytes.** *A*, H4IIEC3 cells were incubated in the presence or absence of palmitate (*Pal*) and antioxidants for 16 h. Total cell lysates were resolved by SDS-PAGE, transferred to a PVDF membrane, and immunoblotted with the indicated antibodies. Detection was by enhanced chemiluminescence. Representative blots are shown. *B*, the values from densitometry of four (NAC or α-tocopherol) independent experiments were normalized to the level of total JNK protein and expressed as the mean -fold increase over control ± S.E. **, $p < 0.01$ *versus* palmitate treatment alone. *Toc*, α-tocopherol.

plies the mitochondrial respiratory chain with electrons. Large amounts of electrons entering the respiratory chain may cause abnormal reduction of oxygen, leading to ROS production. Thus, we next examined whether palmitate-induced ROS production was dependent on mitochondrial fatty acid β-oxidation. CPT-1a (carnitine palmitoyltransferase-1a) is the rate-limiting enzyme in mitochondrial fatty acid β-oxidation. As expected, etomoxir, a CPT-1 inhibitor, decreased palmitate-induced ROS production, by 80% (Fig. 9*A*). Furthermore, palmitate, but not oleate, significantly increased expression of the *CPT-1a* gene (Fig. 9*B*). This up-regulation may contribute to palmitate-induced ROS overproduction, because the accelerated β-oxidation should cause excessive electron flux in the respiratory chain.

DISCUSSION

In the present study, we investigated the direct action of fatty acids on insulin signaling in hepatocytes. The saturated fatty acid palmitate, but not the unsaturated fatty acid oleate, impaired insulin-induced tyrosine phosphorylation of IRS-2, serine phosphorylation of Akt, and serine phosphorylation of GSK-3α, all of which are indicative of insulin resistance in cultured H4IIEC3 hepatocytes (Fig. 10). Unlike *in vivo* findings (6), the expression of the *SREBP-1c* gene was down-regulated by adding palmitate to cultured H4IIEC3 hepatocytes, which is likely a result of a negative feedback loop for fatty acid synthesis, and IRS-2 protein levels were unaffected. FFA-induced insulin resistance has been reported in other insulin-sensitive cells, such as adipocytes (18) and skeletal muscle cells (26). These studies, together with the present results, suggest that FFA inhibits insulin signaling at the level of tyrosine phosphorylation of IRSs, regardless of cell type. Similar to the findings in 3T3-L1 adipocytes (18) and primary mouse hepatocytes and pancreatic β-cells (16), the activation of JNK, a known suppressor of the tyrosine phosphorylation of IRSs, was involved in FFA-induced tyrosine phosphorylation of IRS-2 in cultured H4IIEC3 hepatocytes. Because a JNK inhibitor, SP600125, largely restored palmitate-induced impairment of the insulin signaling pathway, JNK activation seems to play a major role in the development of palmitate-induced insulin resistance in H4IIEC3 hepatocytes. Our results support *in vivo* findings that JNK is activated in the liver of an animal model of obesity and diabetes in which FFA influx into the liver is elevated (9, 27). The overexpression of JNK in mouse liver resulted in hepatic insulin resistance at the level of IRS tyrosine phosphorylation, and the overexpression of a dominant negative mutant of JNK in the liver accelerated hepatic insulin signaling (17).

Given that JNK is activated by many types of cellular stresses (28), we next searched for a link between palmitate treatment and JNK activation in H4IIEC3 hepatocytes. ER stress was unlikely to mediate palmitate-induced insulin resistance in H4IIEC3 hepatocytes, because palmitate caused insulin resistance independent of ER stress, whereas tunicamycin caused ER stress without affecting insulin action. Instead, we found that palmitate-induced ROS generation mediated insulin resistance. ROS are one of many factors suggested to have a possible role in insulin resistance (29, 30). ROS include reactive products, such as superoxide anion, hydrogen peroxide, and

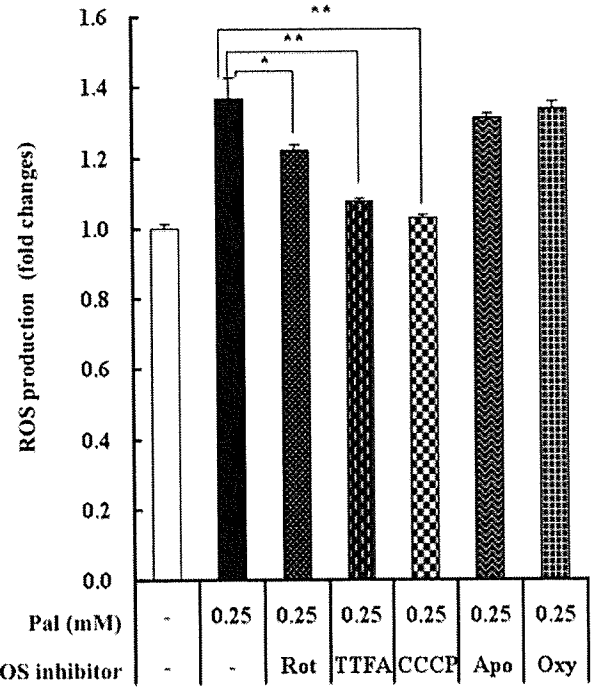

FIGURE 8. **Effects of ROS-producing pathway inhibitors on palmitate-induced ROS production in H4IIEC3 hepatocytes.** H4IIEC3 cells were incubated in the presence or absence of palmitate (*Pal*) and each ROS-producing pathway inhibitor for 8 h. Intracellular ROS production was quantified using the fluorescent probe H_2DCFDA. The values are expressed as mean -fold increase over control ± S.E. ($n = 4$). *, $p < 0.05$ *versus* palmitate treatment alone. **, $p < 0.01$ *versus* palmitate treatment alone. *Rot*, rotenone; *Apo*, apocynin; *Oxy*, oxypurinol; *TTFA*, thenoyltrifluoroacetone; *CCCP*, carbonyl cyanide *m*-chlorophenylhydrazone.

hydroxyl radical, which are formed as by-products of mitochondrial oxidative phosphorylation (OXPHOS). Thus, as a rule, increased mitochondrial OXPHOS flux leads to increased formation of ROS (31, 32). ROS can also be produced during β-oxidation of fatty acids, especially as a by-product of peroxisomal acyl-CoA oxidase activity (32). Additionally, ROS can be produced by dedicated enzymes, such as NADPH oxidase (33), present in phagocytic cells, where ROS are an important part of cellular defense mechanisms. Using specific inhibitors of subcellular ROS, we identified mitochondrial OXPHOS as an important source of palmitate-induced ROS generation in H4IIEC3 hepatocytes. FFAs supply mitochondrial OXPHOS with electrons through mitochondrial fatty acid β-oxidation. A final metabolite of fatty acids, acetyl-CoA, is metabolized in the trichloroacetic acid cycle. In the processes of fatty acid β-oxidation and the trichloroacetic acid cycle, NADH and $FADH_2$ are generated and could supply excessive electrons for OXPHOS.

NAC, a scavenger of ROS, dose-dependently restored glutathione in palmitate-treated cells (supplemental Fig. 5). However, glutathione restoration by NAC was unable to completely rescue palmitate-induced insulin resistance. Furthermore, the combination of NAC and α-tocopherol did not completely reverse JNK activation (supplemental Fig. 6, *A* and *B*) and only partly rescued palmitate-induced insulin resistance (supplemental Fig. 7, *A* and *B*). Therefore, other mechanisms may also be involved in insulin resistance caused by palmitate.

De novo ceramide synthesis is a potential pathway contributing to palmitate-induced JNK activation. Ceramide derived from saturated fatty acids has been reported to activate JNK and inhibit insulin-induced Akt phosphorylation in myocytes (34–36). In our investigation, palmitate increased the intracellular content of ceramide in H4IIEC3 hepatocytes (supplemental Fig. 8). Unfortunately, even at the maximum myriosin concentration, the intracellular accumulation of ceramide was not blocked by myriosin, a potent inhibitor of serine palmitoyltransferase at the first step in ceramide biosynthesis (supplemental Fig. 8). Furthermore, ceramide accumulation was not blocked when myriosin was used in combination with fumonisin B1, an inhibitor of ceramide synthase (data not shown). Therefore, we cannot rule out the possibility that intracellular ceramide contributes to palmitate-induced insulin resistance in H4IIEC3 hepatocytes. Further studies are required to assess the role of the

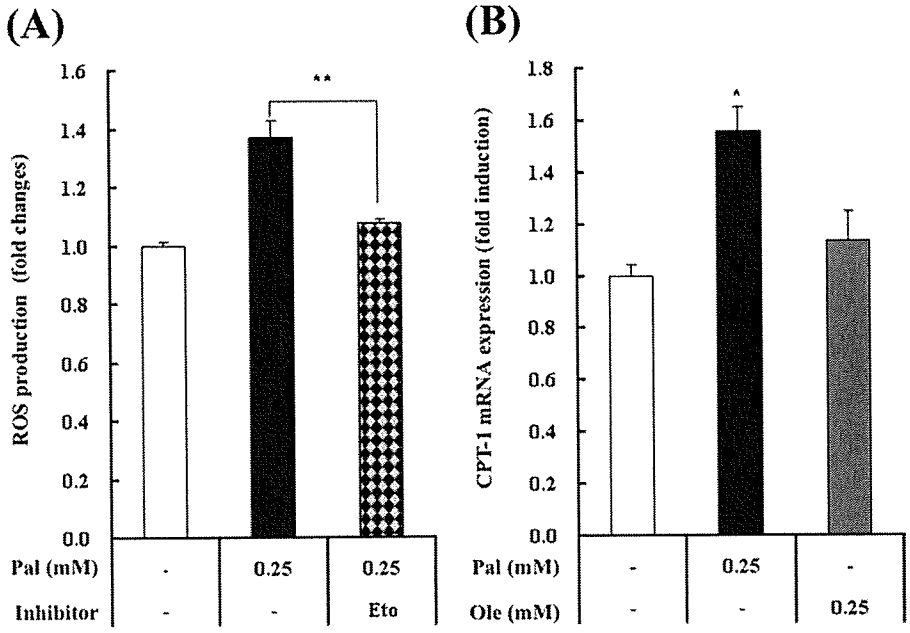

FIGURE 9. **Involvement of mitochondrial fatty acid oxidation in palmitate-induced ROS production.** *A*, H4IIEC3 cells were incubated in the presence or absence of palmitate (*Pal*) and the CPT-1 inhibitor etomoxir (*Eto*) for 8 h. Intracellular ROS production was quantified using the fluorescent probe H_2DCFDA. The values are expressed as mean -fold increase over control ± S.E. ($n = 4$). *B*, H4IIEC3 cells were incubated in the presence or absence of palmitate (*Pal*) or oleate (*Ole*) for 16 h. Total RNA was extracted and subjected to reverse transcription. Using the cDNA as a template, the amounts of CPT-1 mRNA were detected by real time PCR. The values were normalized to the level of 18 S ribosomal RNA and expressed as mean -fold increase over control ± S.E. ($n = 3$). *, $p < 0.05$ *versus* control. **, $p < 0.01$ *versus* palmitate treatment alone.

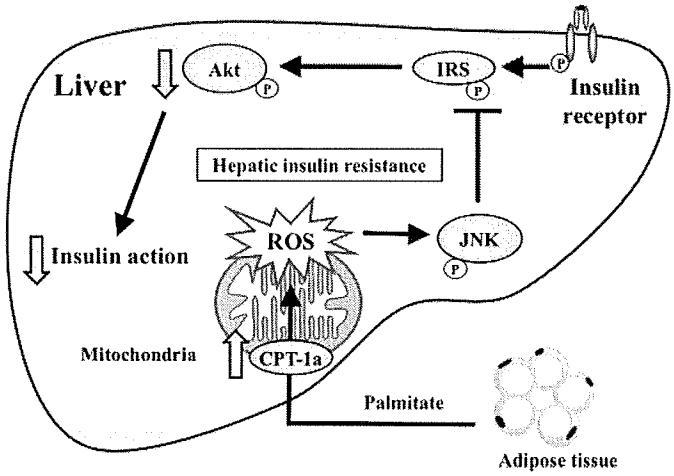

FIGURE 10. **Proposed model for palmitate-induced hepatic insulin resistance.**

ceramide pathway in palmitate-induced insulin resistance in hepatocytes.

In the present study, etomoxir, an inhibitor of CPT-1, decreased palmitate-induced intracellular ROS production. Additionally, palmitate, but not oleate, significantly increased the expression of the *CPT-1a* gene, which may account for the observed differences in insulin action between palmitate and oleate.

Recently, it was reported that fatty acid composition may be a determinant in insulin sensitivity (37, 38). In this regard, we investigated the effect of oleate on insulin signaling in palmitate-treated hepatocytes. Surprisingly, oleate dose-dependently reversed palmitate-induced ROS generation and JNK phosphorylation and rescued palmitate-induced phosphorylation of Akt.[3] Further investigations aimed at elucidating the molecular basis underlying the differential roles and interactions of FFAs are required.

In conclusion, this study identified mitochondrial ROS generation as a critical factor in palmitate-induced hepatic insulin resistance. Palmitate may induce CPT-1 expression, accelerate metabolism, supply excess electrons for mitochondrial OXPHOS, and generate ROS. ROS then desensitize the insulin signaling pathway by activating JNK, impairing tyrosine phosphorylation of IRS-2, and causing hepatic insulin resistance (Fig. 10). The results suggest that an initial event in high fat/sucrose diet-induced or obesity-induced insulin resistance in the liver is mitochondrial ROS generation, which could potentially be a therapeutic target. In addition to previously suggested JNK inhibitors or antioxidants, mitochondrial uncouplers, such as cyanide *m*-chlorophenylhydrazone, may provide a candidate therapeutic strategy for this pathway by preventing ROS generation.

Acknowledgments—We thank Drs. Isao Usui and Hajime Ishihara and Prof. Toshiyasu Sasaoka (Toyama University) for supplying technical expertise on Western blot analysis of phosphoproteins.

[3] H. Takayama and T. Takamura, unpublished data.

REFERENCES

1. Saltiel, A. R., and Kahn, C. R. (2001) *Nature* **414,** 799–806
2. Ota, T., Takamura, T., Kurita, S., Matsuzawa, N., Kita, Y., Uno, M., Akahori, H., Misu, H., Sakurai, M., Zen, Y., Nakanuma, Y., and Kaneko, S. (2007) *Gastroenterology* **132,** 282–293
3. Matsuzawa, N., Takamura, T., Kurita, S., Misu, H., Ota, T., Ando, H., Yokoyama, M., Honda, M., Zen, Y., Nakanuma, Y., Miyamoto, K., and Kaneko, S. (2007) *Hepatology* **46,** 1392–1403
4. Sakurai, M., Takamura, T., Ota, T., Ando, H., Akahori, H., Kaji, K., Sasaki, M., Nakanuma, Y., Miura, K., and Kaneko, S. (2007) *J. Gastroenterol.* **42,** 312–317
5. Boden, G. (1997) *Diabetes* **46,** 3–10
6. Ide, T., Shimano, H., Yahagi, N., Matsuzaka, T., Nakakuki, M., Yamamoto, T., Nakagawa, Y., Takahashi, A., Suzuki, H., Sone, H., Toyoshima, H., Fukamizu, A., and Yamada, N. (2004) *Nat. Cell Biol.* **6,** 351–357
7. Hirosumi, J., Tuncman, G., Chang, L., Gorgun, C. Z., Uysal, K. T., Maeda, K., Karin, M., and Hotamisligil, G. S. (2002) *Nature* **420,** 333–336
8. Boden, G., She, P., Mozzoli, M., Cheung, P., Gumireddy, K., Reddy, P., Xiang, X., Luo, Z., and Ruderman, N. (2005) *Diabetes* **54,** 3458–3465
9. Ozcan, U., Cao, Q., Yilmaz, E., Lee, A. H., Iwakoshi, N. N., Ozdelen, E., Tuncman, G., Gorgun, C., Glimcher, L. H., and Hotamisligil, G. S. (2004) *Science* **306,** 457–461
10. Kim, J. K., Fillmore, J. J., Chen, Y., Yu, C., Moore, I. K., Pypaert, M., Lutz, E. P., Kako, Y., Velez-Carrasco, W., Goldberg, I. J., Breslow, J. L., and Shulman, G. I. (2001) *Proc. Natl. Acad. Sci. U. S. A.* **98,** 7522–7527
11. Turinsky, J., O'Sullivan, D. M., and Bayly, B. P. (1990) *J. Biol. Chem.* **265,** 16880–16885
12. Du, K., Herzig, S., Kulkarni, R. N., and Montminy, M. (2003) *Science* **300,** 1574–1577
13. Nishikawa, T., Edelstein, D., Du, X. L., Yamagishi, S., Matsumura, T., Kaneda, Y., Yorek, M. A., Beebe, D., Oates, P. J., Hammes, H. P., Giardino, I., and Brownlee, M. (2000) *Nature* **404,** 787–790
14. Matsuzawa-Nagata, N., Takamura, T., Ando, H., Nakamura, S., Kurita, S., Misu, H., Ota, T., Yokoyama, M., Honda, M., Miyamoto, K., and Kaneko, S. (2008) *Metabolism* **57,** 1071–1077
15. Aguirre, V., Uchida, T., Yenush, L., Davis, R., and White, M. F. (2000) *J. Biol. Chem.* **275,** 9047–9054
16. Solinas, G., Naugler, W., Galimi, F., Lee, M. S., and Karin, M. (2006) *Proc. Natl. Acad. Sci. U. S. A.* **103,** 16454–16459
17. Nakatani, Y., Kaneto, H., Kawamori, D., Hatazaki, M., Miyatsuka, T., Matsuoka, T. A., Kajimoto, Y., Matsuhisa, M., Yamasaki, Y., and Hori, M. (2004) *J. Biol. Chem.* **279,** 45803–45809
18. Nguyen, M. T., Satoh, H., Favelyukis, S., Babendure, J. L., Imamura, T., Sbodio, J. I., Zalevsky, J., Dahiyat, B. I., Chi, N. W., and Olefsky, J. M. (2005) *J. Biol. Chem.* **280,** 35361–35371
19. Bennett, B. L., Sasaki, D. T., Murray, B. W., O'Leary, E. C., Sakata, S. T., Xu, W., Leisten, J. C., Motiwala, A., Pierce, S., Satoh, Y., Bhagwat, S. S., Manning, A. M., and Anderson, D. W. (2001) *Proc. Natl. Acad. Sci. U. S. A.* **98,** 13681–13686
20. Karaskov, E., Scott, C., Zhang, L., Teodoro, T., Ravazzola, M., and Volchuk, A. (2006) *Endocrinology* **147,** 3398–3407
21. Harding, H. P., Calfon, M., Urano, F., Novoa, I., and Ron, D. (2002) *Annu. Rev. Cell Dev. Biol.* **18,** 575–599
22. Kaneto, H., Kawamori, D., Nakatani, Y., Gorogawa, S., and Matsuoka, T. A. (2004) *Drug News Perspect.* **17,** 447–453
23. Furukawa, S., Fujita, T., Shimabukuro, M., Iwaki, M., Yamada, Y., Nakajima, Y., Nakayama, O., Makishima, M., Matsuda, M., and Shimomura, I. (2004) *J. Clin. Invest.* **114,** 1752–1761
24. Carlsson, C., Borg, L. A., and Welsh, N. (1999) *Endocrinology* **140,** 3422–3428
25. Miller, T. A., LeBrasseur, N. K., Cote, G. M., Trucillo, M. P., Pimentel, D. R., Ido, Y., Ruderman, N. B., and Sawyer, D. B. (2005) *Biochem. Biophys. Res. Commun.* **336,** 309–315
26. Chavez, J. A., and Summers, S. A. (2003) *Arch. Biochem. Biophys.* **419,** 101–109
27. Nakatani, Y., Kaneto, H., Kawamori, D., Yoshiuchi, K., Hatazaki, M., Mat-

suoka, T. A., Ozawa, K., Ogawa, S., Hori, M., Yamasaki, Y., and Matsuhisa, M. (2005) *J. Biol. Chem.* **280,** 847–851
28. Davis, R. J. (2000) *Cell* **103,** 239–252
29. Evans, J. L., Goldfine, I. D., Maddux, B. A., and Grodsky, G. M. (2002) *Endocr. Rev.* **23,** 599–622
30. Houstis, N., Rosen, E. D., and Lander, E. S. (2006) *Nature* **440,** 944–948
31. Brownlee, M. (2001) *Nature* **414,** 813–820
32. Osmundsen, H., Bremer, J., and Pedersen, J. I. (1991) *Biochim. Biophys. Acta* **1085,** 141–158
33. De Minicis, S., Bataller, R., and Brenner, D. A. (2006) *Gastroenterology* **131,** 272–275
34. Chavez, J. A., Knotts, T. A., Wang, L. P., Li, G., Dobrowsky, R. T., Florant, G. L., and Summers, S. A. (2003) *J. Biol. Chem.* **278,** 10297–10303
35. Powell, D. J., Turban, S., Gray, A., Hajduch, E., and Hundal, H. S. (2004) *Biochem. J.* **382,** 619–629
36. Schmitz-Peiffer, C., Craig, D. L., and Biden, T. J. (1999) *J. Biol. Chem.* **274,** 24202–24210
37. Bruce, C. R., and Febbraio, M. A. (2007) *Nat. Med.* **13,** 1137–1138
38. Cao, H., Gerhold, K., Mayers, J. R., Wiest, M. M., Watkins, S. M., and Hotamisligil, G. S. (2008) *Cell* **134,** 933–944

Biochemical and Biophysical Research Communications 380 (2009) 684–688

Contents lists available at ScienceDirect

Biochemical and Biophysical Research Communications

journal homepage: www.elsevier.com/locate/ybbrc

The hepatic circadian clock is preserved in a lipid-induced mouse model of non-alcoholic steatohepatitis

Hitoshi Ando [a,b], Toshinari Takamura [a,*], Naoto Matsuzawa-Nagata [a], Kosuke R. Shima [a], Seiji Nakamura [a], Masafumi Kumazaki [a], Seiichiro Kurita [a], Hirofumi Misu [a], Naoyuki Togawa [c], Tatsunobu Fukushima [c], Akio Fujimura [b], Shuichi Kaneko [a]

[a] Department of Disease Control and Homeostasis, Kanazawa University Graduate School of Medical Science, 13-1 Takara-machi, Kanazawa, Ishikawa 920-8641, Japan
[b] Division of Clinical Pharmacology, Department of Pharmacology, School of Medicine, Jichi Medical University, Shimotsuke, Tochigi 329-0498, Japan
[c] Yokohama Research Laboratories, Mitsubishi Rayon Co., Ltd, Yokohama, Kanagawa 230-0053, Japan

ARTICLE INFO

Article history:
Received 21 January 2009
Available online 29 January 2009

Keywords:
Atherogenic diet
Circadian rhythm
Clock gene
Non-alcoholic steatohepatitis
Oxidative stress

ABSTRACT

Recent studies have correlated metabolic diseases, such as metabolic syndrome and non-alcoholic fatty liver disease, with the circadian clock. However, whether such metabolic changes *per se* affect the circadian clock remains controversial. To address this, we investigated the daily mRNA expression profiles of clock genes in the liver of a dietary mouse model of non-alcoholic steatohepatitis (NASH) using a custom-made, high-precision DNA chip. C57BL/6J mice fed an atherogenic diet for 5 weeks developed hypercholesterolemia, oxidative stress, and NASH. DNA chip analyses revealed that the atherogenic diet had a great influence on the mRNA expression of a wide range of genes linked to mitochondrial energy production, redox regulation, and carbohydrate and lipid metabolism. However, the rhythmic mRNA expression of the clock genes in the liver remained intact. Most of the circadianly expressed genes also showed 24-h rhythmicity. These findings suggest that the biological clock is protected against such a metabolic derangement as NASH.

Various behavioral and physiological processes, including feeding behavior and energy metabolism, exhibit circadian (i.e., 24-h) rhythmicity, which may play a role in maintaining functional homeostasis. Recent studies have revealed that the circadian clock system consists essentially of a set of clock genes [1,2]. In mammals, the circadian clock resides in the hypothalamic suprachiasmatic nucleus (SCN), which is recognized as being the master clock, and in almost all peripheral tissues [3]. The SCN appears to coordinate peripheral clocks, because it is not essential for driving peripheral oscillations [3].

Rhythmic transcriptional enhancement by two basic helix–loop–helix transcription factors, CLOCK and brain and muscle Arnt-like protein 1 (BMAL1), provides the basic drive for the intracellular clock [1,2]. In parallel, the heterodimer activates the transcription of various clock-controlled genes. Given that some clock-controlled genes also serve as transcription factors, the expression of numerous genes may be tied to the functions of the circadian clock [1,2]. For example, nearly half of the known nuclear receptors, including peroxisome proliferator-activated receptors (α, γ, δ) and thyroid hormone receptors (α, β), exhibit circadian expression in liver and adipose tissues, providing a possible explanation for the cyclical behavior of carbohydrate and lipid metabolism [4].

Recent studies have demonstrated relationships between circadian clock function and the development of metabolic diseases, such as type 2 diabetes, metabolic syndrome, and non-alcoholic fatty liver disease (NAFLD). In mice, homozygous mutations in the *Clock* gene lead to the development of metabolic syndrome [5]. Moreover, we showed that the rhythmic expression of clock genes is blunted in the liver and visceral adipose tissues in KK-A^y mice, a genetic model of obese diabetes [6]. In humans, a similar effect in type 2 diabetes was found in peripheral leukocytes [7]. Furthermore, genetic variations in the *BMAL1* gene are associated with susceptibility to type 2 diabetes and hypertension [8], and *CLOCK* haplotypes are associated with metabolic syndrome [9] and NAFLD [10]. Thus, impairment of the circadian clock appears to contribute to the development of metabolic diseases.

However, whether metabolic diseases *per se* affect the circadian clock remains controversial. High glucose down-regulates mRNA expression of the clock genes (*Per1* and *Per2*) in cultured fibroblasts [11]. Additionally, the DNA-binding activity of the CLOCK-BMAL1 heterodimer is regulated by the redox state, at least *in vitro* [12]. Kohsaka et al. [13] reported that a high-fat diet affected the rhythmic mRNA expression of *Clock*, *Bmal1*, and *Per2* in the liver and adipose tissues of mice. Considering these findings, alterations in

* Corresponding author. Fax: +81 76 234 4250.
E-mail address: ttakamura@m-kanazawa.jp (T. Takamura).

0006-291X/$ - see front matter © 2009 Elsevier Inc. All rights reserved.
doi:10.1016/j.bbrc.2009.01.150

glucose, lipid, and energy metabolism; redox state; and/or the concentrations of humoral factors, such as plasma glucose, appear to influence the peripheral circadian clock. However, Oishi et al. [14] demonstrated that clock function was preserved, to a large degree, in the livers, hearts, and kidneys of mice with streptozotocin-induced insulinopenic diabetes. We also revealed that the circadian clock is hardly impaired in the liver and adipose tissues of non-obese, mild hyperglycemic Goto-Kakizaki rats [15]. Furthermore, we did not observe impairment of the circadian clock in the liver or adipose tissues of mice fed a high-fat diet, even though the mice developed metabolic syndrome, characterized by obesity, hyperlipidemia, and hyperglycemia [16]. Although the reasons for these discrepancies among the various studies are unknown, one reason might be differences in the severity of the pathological condition.

Non-alcoholic steatohepatitis (NASH) is an aggressive form of NAFLD, and the liver with steatosis and inflammation develops hepatic insulin resistance, lipotoxicity, oxidative stress, and mitochondrial abnormalities, which lead to hepatic fibrosis or cirrhosis [17]. We recently established a mouse model of NASH, induced by feeding an atherogenic diet [18]. In this model, the atherogenic diet induced steatosis, inflammation, cellular ballooning, stellate cell activation, hepatic insulin resistance, lipid peroxidation, and oxidative stress in the liver; it finally caused hepatic cirrhosis. Thus, the pathological conditions in the liver of this model are complex and quite severe compared with those of mice fed a simple high-fat diet [13,16]. Therefore, it is reasonable to expect that the hepatic circadian clock may be impaired in this model, if the alterations in metabolism and redox state affect the oscillator. To test this, we developed a custom-made, high-precision DNA chip useful for analyzing the metabolic status of the liver and investigated the rhythmic mRNA expression of clock genes and genes linked to carbohydrate and lipid metabolism, energy production, and redox regulation in the livers of mice fed an atherogenic diet.

Materials and methods

Mice. Male C57BL/6J mice (Charles River Laboratories Japan, Yokohama, Japan) were obtained at 5 weeks of age and maintained under conditions of controlled temperature and humidity and a 12-h light (08:45–20:45 h)/12-h dark (20:45–08:45 h) cycle. Mice had free access to food and drinking water. After 3 days of acclimation, the mice were divided into two groups. Half of the mice ($n = 16$) were fed a standard laboratory diet (CRF-1, Oriental Yeast Co., Tokyo, Japan), whereas the others ($n = 16$) were given an atherogenic diet (Research Diets, New Brunswick, NJ) containing 34.3% fat (lard, soybean oil), 25.8% protein (casein, L-cystine), 24.6% carbohydrate (maltodextrin, sucrose), 1.3% cholesterol, 0.5% sodium cholate, 5.7% mineral mixture, 1.5% vitamin mixture, and 6.3% cellulose. After 5 weeks of feeding, animals were sacrificed to obtain blood and liver samples at the following zeitgeber times (ZT): 0, 6, 12, and 18, in which ZT 0 is defined as lights on and ZT 12 as lights off.

All animal procedures were performed in accordance with the standards set forth in the Guidelines for the Care and Use of Laboratory Animals at the Takara-machi campus of Kanazawa University (Kanazawa, Japan).

Statistical analyses. Differences in the variables and mRNA levels between mice fed the atherogenic diet and control mice were evaluated using Student's t test. The rhythmicity of each gene was assessed using one-way ANOVA. The values are presented as the means ± SEM, and $P < 0.05$ was deemed to indicate statistical significance. All calculations were performed using SPSS software (version 11 for Windows, SPSS Japan, Tokyo, Japan).

Additional details on methods. For details on the blood chemistry, DNA chip analysis, and real-time quantitative PCR, see Supplemental Materials and methods.

Results

Development of a custom-made DNA chip suitable for metabolic research

We established a database of hepatic gene expression profiles in various human diseases, and rodent models of diabetes and/or obesity. The models include patients with type 2 diabetes, with or without obesity [19–24] and NAFLD [25]; genetic rodent models of type 2 diabetes and/or obesity [6,26]; diet-induced rodent models of obesity [27]; diet-induced rodent models of NAFLD [18,28,29]; and a rodent model of ischemic heart disease (manuscript submitted). We extracted the significantly altered genes in each metabolic pathway both in human diseases and animal models and selected 190 mouse genes linked to the circadian clock, energy production, redox regulation, ROS defense, MAPK cascade, energy and cholesterol metabolism, and protein degradation. Because expression of 70 of these genes was hardly detected in a liver sample (FirstChoice mouse liver total RNA, Applied Biosystems) or was determined differently from the results analyzed by real-time PCR, we used data for the other 120 genes for analyses in this study (Supplemental Table 1). The results of the 120 genes analyzed by the DNA chip strongly correlated with those obtained by real-time PCR (Pearson's correlation coefficient $r = 0.963$, $P < 0.0001$; Supplemental Fig. 2).

Mouse model of NASH induced by feeding an atherogenic diet

As reported previously [18], mice fed an atherogenic diet for 5 weeks developed NASH, diagnosed based on histology (Supplemental Fig. 3). Serum concentrations of ALT and total cholesterol in mice fed the atherogenic diet were significantly higher than those in control mice (Table 1). The concentration of d-ROMs was also elevated, suggesting that oxidative stress was induced in the mice on the atherogenic diet.

Global gene expression profile in the livers of mice fed an atherogenic diet

Consistent with the histological and biochemical findings, the DNA chip analyses revealed that the atherogenic diet had a wide influence on mRNA expression, affecting genes linked to energy production, redox regulation, ROS defense, the MAPK cascade, nuclear receptors, energy and cholesterol metabolism, and protein degradation (Supplemental Table 2). In most of the genes examined, the atherogenic diet decreased transcript levels. Specifically,

Table 1
Metabolic parameters in mice fed a regular or atherogenic diet.

Parameter	Control	Atherogenic	P
Body weight (g)	28.7 ± 0.8	23.2 ± 0.9	<0.01
Blood glucose (mg/dL)	166 ± 5	163 ± 8	0.73
Serum ALT (U/L)	18 ± 1	51 ± 7	<0.01
Serum total cholesterol (mg/dL)	98 ± 2	151 ± 7	<0.01
Serum HDL-cholesterol (mg/dL)	71 ± 2	71 ± 3	0.90
Serum triglyceride (mg/dL)	80 ± 13	14 ± 2	<0.01
d-ROMs (U)	20 ± 1	34 ± 3	<0.01

Blood samples were obtained from non-fasted mice at zeightgeber time 0 and 12 ($n = 4$ for each time point in both groups).
Data are means ± SEM of eight mice.
ALT, alanine aminotransferase; HDL, high-density lipoprotein; d-ROMs, derivatives of reactive oxygen metabolites.